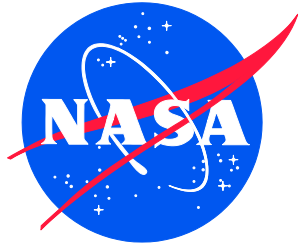# NESC Peer Review of Exploration Systems Development (ESD) Integrated Vehicle Modal Test, Model Correlation, Development Flight Instrumentation (DFI) and Flight Loads Readiness

Uncertainty Propagation for Model Validation Sub-task

Joel Sills/NESC
Langley Research Center, Hampton, Virginia

Paul Blelloch and Daniel Kammer
ATA Engineering, Herndon, Virginia

NASA STI Program Report Series

Since its founding, NASA has been dedicated to the advancement of aeronautics and space science. The NASA scientific and technical information (STI) program plays a key part in helping NASA maintain this important role.

The NASA STI program operates under the auspices of the Agency Chief Information Officer. It collects, organizes, provides for archiving, and disseminates NASA's STI. The NASA STI program provides access to the NTRS Registered and its public interface, the NASA Technical Reports Server, thus providing one of the largest collections of aeronautical and space science STI in the world. Results are published in both non-NASA channels and by NASA in the NASA STI Report Series, which includes the following report types:

- TECHNICAL PUBLICATION. Reports of completed research or a major significant phase of research that present the results of NASA Programs and include extensive data or theoretical analysis. Includes compilations of significant scientific and technical data and information deemed to be of continuing reference value. NASA counterpart of peer-reviewed formal professional papers but has less stringent limitations on manuscript length and extent of graphic presentations.

- TECHNICAL MEMORANDUM. Scientific and technical findings that are preliminary or of specialized interest, e.g., quick release reports, working papers, and bibliographies that contain minimal annotation. Does not contain extensive analysis.

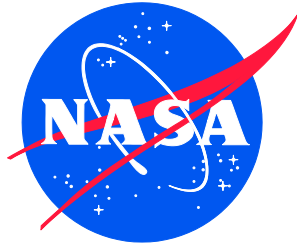- CONTRACTOR REPORT. Scientific and technical findings by NASA-sponsored contractors and grantees.

- CONFERENCE PUBLICATION. Collected papers from scientific and technical conferences, symposia, seminars, or other meetings sponsored or co-sponsored by NASA.

- SPECIAL PUBLICATION. Scientific, technical, or historical information from NASA programs, projects, and missions, often concerned with subjects having substantial public interest.

- TECHNICAL TRANSLATION. English-language translations of foreign scientific and technical material pertinent to NASA's mission.

Specialized services also include organizing and publishing research results, distributing specialized research announcements and feeds, providing information desk and personal search support, and enabling data exchange services.

For more information about the NASA STI program, see the following:

- Access the NASA STI program home page at http://www.sti.nasa.gov

- Help desk contact information:

https://www.sti.nasa.gov/sti-contact-form/
and select the "General" help request type.

NASA/TM–20210009733
NESC-RP-16-01110

NESC Peer Review of Exploration Systems Development (ESD) Integrated Vehicle Modal Test, Model Correlation, Development Flight Instrumentation (DFI) and Flight Loads Readiness

Uncertainty Propagation for Model Validation Sub-task

Joel Sills/NESC
Langley Research Center, Hampton, Virginia

Paul Blelloch and Daniel Kammer
ATA Engineering, Herndon, Virginia

February 2021

Acknowledgments

Available from:

NASA STI Program / Mail Stop 148
NASA Langley Research Center
Hampton, VA 23681-2199
Fax: 757-864-6500

NASA Engineering and Safety Center
Technical Assessment Report

NESC Peer Review of Exploration Systems Development (ESD) Integrated Vehicle Modal Test, Model Correlation, Development Flight Instrumentation (DFI) and Flight Loads Readiness

Uncertainty Propagation for Model Validation Sub-task

January 28, 2021

Report Approval and Revision History

NOTE: This document was approved at the January 28, 2021, NRB. This document was submitted to the NESC Director on January 29, 2021, for configuration control.

Approved:	*Original Signature on File*	1/29/21
	NESC Director	Date

Version	Description of Revision	Office of Primary Responsibility	Effective Date
1.0	Initial Release	Joel Sills, NASA Deputy Technical Fellow for Loads and Dynamics, JSC	01/28/2021
1.1	ITAR and distribution limitation restrictions removed per Export Control office and assessment lead.	Joel Sills, NASA Deputy Technical Fellow for Loads and Dynamics, JSC	02/10/2021

Table of Contents

List of Figures

List of Tables

Technical Assessment Report

1.0   Notification and Authorization

This assessment is part of a multi-year activity that spans the complete development of the Space Launch Systems (SLS) integrated vehicle structural dynamic models, and the development of the certification of flight readiness for the Artemis I (formerly Exploration Mission 1 (EM-1)) and Artemis II vehicles, and their variants. It is modeled after the scope and execution of the Multipurpose Crew Vehicle (MPCV) Aerodynamic/Aerothermal Database Models and Methods Peer Review assessment (TI-05-177-E) and the SLS Aerosciences Independent Consultation and Review (TI-12-00834), which have proven to be efficient and beneficial to the program and to NASA.

This assessment sub-task was requested by the Exploration Systems Division (ESD/Cross-program Systems Integration (CSI)) loads, dynamics, and environments lead to provide the Agency, SLS, Exploration Ground Systems (EGS), and MPCV Programs with an alternate method, besides the SLS Program's Best Model Estimate method and Flight Dynamic Risk Assessment process, for assessing the uncertainty from each building block test to a projection of the overall integrated system uncertainty.

The key stakeholders for this assessment are the Human Exploration and Operations Mission Directorate (HEOMD) chief engineer; the EGS, MPCV, and SLS Programs and their respective chief engineers; the Joint Loads Task Team (JLTT) co-chairs; the Cross-program Integration Team (CPIT); and NASA ESD. The specific stakeholders are:

JLTT
- Mr. James Booker, SLS Program, Chair
- Mr. Chris Brown, EGS Program, Co-chair
- Ms. Quyen Jones, MPCV Program, Co-chair
- Dr. Patrick Hull, Marshall Space Flight Center (MSFC); SLS Program, Dynamic Test and Model Sensitivity Study (DTaMSS) lead

Program Chief Engineers
- Mr. John Mcmanamen, HEOMD Chief Engineer for ESD
- Mr. Chuck Dingell, MPCV Program
- Dr. John Blevins, SLS Program
- Mr. Greg Horvath, EGS Program

CPIT
- Mr. Wayne Jermstad, Ms. Dawn Stanley, and Mr. George Deckert, ESD
- Mr. Kirk Lougheed, EGS Program
- Mr. Brian McDonald, MPCV Program
- Mr. Andy Warren, SLS Program

2.0   Signature Page

Submitted by:

Team Signature Page on File – 2/1/21

—————————————————————
Mr. Joel Sills   Date

Significant Contributors:

—————————————————————   —————————————————————
Dr. Paul Blelloch   Date   Dr. Daniel Kammer   Date

Signatories declare the findings, observations, and NESC recommendations compiled in the report are factually based from data extracted from program/project documents, contractor reports, and open literature, and/or generated from independently conducted tests, analyses, and inspections.

3.0   Team List

Name	Discipline	Organization
Core Team		
Joel Sills	NESC Lead	JSC
Dexter Johnson	Technical Lead	GRC
Paul Blelloch	Large Systems Modeling and Advanced Dynamic Analysis and Uncertainty Quantification (UQ)/Loads and Dynamics (L&D) Technical Discipline Team (TDT)	ATA Engineering
Daniel Kammer	Modal Analysis and Test Correlation and UQ/L&D TDT	ATA Engineering
Business Management		
John LaNeave	Program Analyst	LaRC/MTSO
Assessment Support		
Melinda Meredith	Project Coordinator	LaRC/AMA
Linda Burgess	Planning and Control Analyst	LaRC/AMA
Leanna Bullock	Technical Editor	LaRC/AMA

3.1   Acknowledgments

The authors would like to recognize and thank NASA Engineering and Safety Center (NESC) management and NESC Review Board (NRB) members. In addition, the NESC team would like to thank the ESD/CSI leadership and the EGS and SLS engineering personnel for support in providing data and metrics for this assessment.

4.0 Executive Summary

The Space Launch System (SLS) integrated configuration consists of a number of components that are assembled into a launch vehicle (LV)[1]. Finite element models (FEMs) of these components are developed by various contractors and NASA centers, reduced to Hurty/Craig-Bampton (HCB) models, and assembled to represent the flexible body characteristics of the SLS integrated system. The assembled models are used for control system stability and performance analysis, coupled loads analysis (CLA), and pogo stability analysis. Figure 4.0-1 shows an image of the SLS in prelaunch configuration.

Figure 4.0-1. SLS in Prelaunch Configuration

Historically, NASA has tested LVs in an integrated configuration with boundary conditions controlled to approximate the boundary conditions expected in flight. Integrated Vehicle Ground Vibration Tests (IVGVT) increase confidence that structural loads predicted using system FEMs are within specified limits with respect to accuracy and uncertainty. However, to minimize cost and schedule, the cross-program decision was made to not perform the IVGVT and rely more heavily on analytical methods supported by component test results. This process is referred to as the "building-block approach," in which system components are tested individually, and component models are correlated and updated to agree with test results to the extent possible.

---

[1] For the purpose of this report, the Space Launch System (SLS) integrated system consists of the Block 1 SLS (i.e., left and right solid rocket boosters (LSRB and RSRB), the core stage (CS), and the interim cryogenic propulsion stage (ICPS)) and Multipurpose Crew Vehicle (MPCV) (i.e., crew module (CM), European service module (ESM), and launch abort system (LAS)). Ground based configurations also include the Mobile Launcher (ML).

However, there will be an integrated system that will undergo testing (i.e., the Integrated Modal Test (IMT)). The test is a ground test of the integrated vehicle, assembled on the Mobile Launcher (ML) in the Vehicle Assembly Building (VAB) facility at Kennedy Space Center (KSC). The results of the IMT will provide an opportunity to validate or update previously correlated SLS component models such that, in an assembled configuration, they provide agreement with integrated system test results.

For this test, the integrated SLS is mounted to the ML at the base of the solid rocket boosters with the Multipurpose Crew Vehicle (MPCV) replaced by the Mass Simulator for Orion (MSO). The IMT/MSO, shown in Figure 4.0-2, is resting on the six VAB support posts with no Crawler Transporter. The initial analytical model used in this assessment consists of SLS HCB components developed based on the IMT R3A integrated FEM provided by Marshall Space Flight Center (MSFC) Structural Dynamics & Integration Branch, except for the Flight Readiness Analysis Cycle (FRAC) version of the Core Stage (CS), which will be used in IMT R4. The Interim Cryogenic Propulsion Stage (ICPS) and CS are empty, with CS pressurization stiffness included corresponding to 4 pounds per square inch (psi). The integrated model was divided into six HCB components including the MSO combined with the MPCV Spacecraft Adaptor (MSA), a combined ICPS and Launch Vehicle Stage Adapter (LVSA), the CS, the left solid rocket booster (LSRB), right solid rocket booster (RSRB), and the ML.
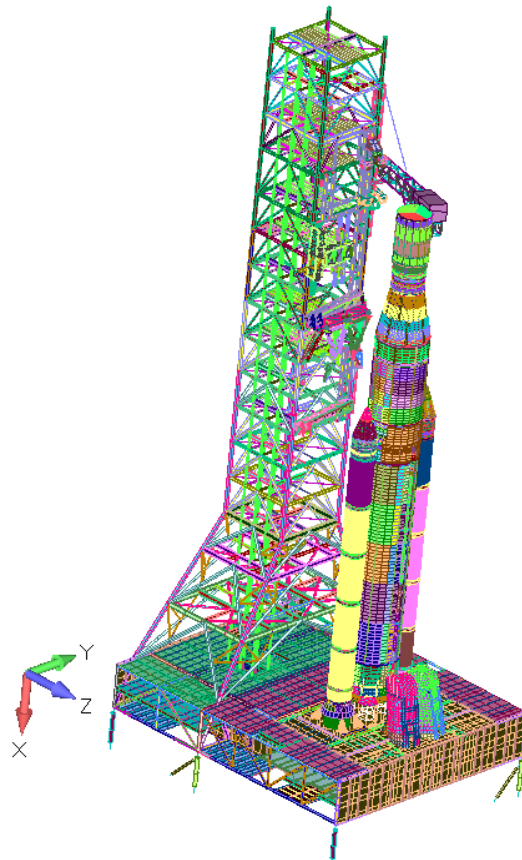
Figure 4.0-2. IMT with MSO on six VAB Mounts[2]

---

[2] Image taken from NESC Review Board Stakeholder Briefing, "Integrated Modal Test (IMT) with Mass Simulator for Orion (MSO) Independent Assessment Task", November 2019.

There is some level of uncertainty in every model, which flows to a level of uncertainty in predicted results. The purpose of uncertainty quantification (UQ) is to provide statistical bounds on prediction accuracy based on model uncertainty. This is distinct from model updating, which attempts to modify models to improve their accuracy. UQ does not improve the accuracy of models but accepts that the models are inaccurate and attempts to quantify the impact of that inaccuracy on predicted results. Previously, a new method for UQ, called the Hybrid Parametric Variation (HPV) method, was applied to SLS HCB components to predict system-level statistics for SLS attitude control transfer functions and CS section loads due to buffet [ref. 1]. The HPV method combines a parametric variation of the HCB fixed interface (FI) modal frequencies with a nonparametric variation (NPV) method that randomly varies the HCB mass and stiffness matrices as Wishart [ref. 2] random matrix distributions using random matrix theory (RMT).

Alternatively, the most common approach for modeling uncertainty in the structural dynamics community is a parametric approach, which varies physical parameters in the model. However, there are several disadvantages associated with the parametric method. Determining a reduced set of parameters that have a significant impact on the system response can be time consuming, and the selected parameter probability distributions are rarely available. In practice, therefore, the parameters are simply surrogates for actual errors, and the link to actual parameter uncertainty is lost. Another major drawback is that the uncertainty that can be represented is limited to the form of the nominal FEM, and the experience of the authors based on numerous aerospace programs is that almost all errors in FEMs are in form rather than parameter values. This fact is supported by the observation of the authors that it is almost never possible to "tune" a FEM to match modal test results by only modifying model parameters. Model-form uncertainty cannot be directly represented by FEM input parameters and cannot be included in a parametric approach. However, model-form uncertainty can be modeled using RMT, where a probability distribution is developed for the matrix ensemble of interest. The major advantage of the NPV method is that it covers errors in model form.

The HPV method anchors uncertainty at the HCB component level to component modal test results by matching HCB modes to test modes based on modal effective mass (MEM) or mode descriptions, and then applying differing levels of frequency variation. The specific variations depend on the degree to which a component FEM has been validated through modal testing. The NPV method is then layered on top of the frequency variation to match modal test cross-orthogonality (XO) results. Once the component uncertainty models are all identified, they are assembled, and the uncertainty is then propagated to the system level using a Monte Carlo (MC) approach that generates statistics for system-level results. This provides a UQ method that can be traced directly to available test data, and which can be updated as additional data and better correlated models become available.

The purpose of this assessment was to apply the HPV UQ approach to the IMT/MSO ground vibration test. Projection of component test-based uncertainty into the system provides estimates of the system-level uncertainty that can be expected in target modal parameters, such as frequencies and mode shapes. Component uncertainty was propagated into system-level frequency response, complex mode indicator functions (CMIF) and normal mode indicator functions (NMIF) [ref. 3]. Statistics for CMIF and NMIF can be used during pretest analysis to determine the probability that the target modes will be adequately excited and measured during the modal test using the proposed sensor and shaker configurations. This assessment was completed prior to the IMT. However, during future posttest analysis, the test results can be

compared to the UQ predictions. If the uncertainty predicted by the UQ analysis covers the test results, then there is increased confidence that the HPV UQ method and the approach used to assign component uncertainty models are valid.

This report presents a brief summary of the theory behind the NPV and HPV methods, and a description of the IMT components and corresponding component uncertainty models, followed by the presentation of MC-based system-level statistics for target modal parameters, selected frequency response functions, and complex- and normal-mode indicator functions. Two cases are considered using the initial R3A-based model, the first includes all the component uncertainty models assigned based on component modal test results, while the second case assumes that there is no uncertainty in the ML model. At the time of this assessment, it was believed the ML was the component with the greatest amount of uncertainty. Model correlation and updating of the ML is still in progress, meaning that the sensor set and shaker locations are still evolving. It has been found that the ability of the shaker configuration to adequately excite the target modes is very dependent on the most recent updated ML model version. Therefore, the statistics presented in this report must be considered as preliminary. It is believed that the two cases considered should bracket reality. MC analysis of the two cases showed that the uncertainty in the ML dominates the uncertainty in the IMT configuration. However, even in the case of high ML uncertainty, the shakers selected at the time of this assessment adequately excited most of the target modes for the selected sensor configuration for most of the random systems in the ensemble.

In order to be more consistent with future IMT test and analysis, a third UQ analysis was performed where the components were upgraded to the FRAC models that comprise the MSFC R4 IMT configuration. In addition, two shakers were added, the target mode set was changed to coincide with the R4 configuration, and the senor set was also updated. The FRAC ML component model was updated considerably over time based on component test results. Therefore, it was believed that while the results of this UQ analysis are not directly comparable to the results of the previous two UQ analyses, the uncertainty in the predicted results should lie somewhere between the uncertainties predicted for the R3A IMT configurations using the pretest Vehicle Analysis Cycle 1 (VAC-1) ML and the certain ML.

The results of this UQ assessment provide meaningful insight into the effects of component uncertainty on system-level results. However, the assessment was not meant to be a comprehensive UQ analysis of the SLS IMT. For simplicity, noteworthy sources of uncertainty, such as component damping, were neglected in this work. In future work, it is believed that the HPV approach should also be applied to the dispersion of the component damping matrix. Finally, while the HPV method provides a valuable tool for complex system UQ analysis using only a limited amount of data, it is believed that confidence in predicted results could be improved through a rigorous validation program.

5.0   Data Analysis

The main body of this report is organized as follows. First, a brief summary of the theory behind the NPV and HPV methods is presented, followed by a description of the IMT components and the identification of their corresponding component uncertainty models. The MC-based system statistics are then presented for target modal parameters, selected frequency response functions, and CMIF and NMIF. At the time of the IMT R3A study, based on test results, it was known that the ML component model had a substantial amount of uncertainty. Two cases were considered for the IMT R3A configuration, the first included all the component uncertainty models assigned based on component modal test results, while the second case assumed that there was no uncertainty in the ML component model. It was found that uncertainty in the ML dominates the uncertainty in the system. During the course of the R3A analysis, the IMT component models were improved to better correlate with test results. This was especially the case for the ML component model. To reflect this evolution, the IMT UQ analysis was repeated for the R4 configuration, which contained the most recent component models. IMT R3A and R4 configuration component models differ substantially, so it can be difficult to directly compare predicted results. However, it is believed that the predicted system uncertainty for R4 should lie somewhere between that predicted for the two R3A cases because the uncertainty in the ML dominates system uncertainty, and ML uncertainty in the R4 configuration lies somewhere between the ML uncertainty in the two R3A cases.

5.1   Theory of the Hybrid Parametric Variation Method

The IMT uncertainty quantification and propagation analysis was performed using the HPV method, which is discussed in detail in Section 5.3 of Reference 1 and in References 4 and 5. A brief summary is presented, and theory corresponding to developments in the method.

The basis for the NPV component of the HPV method is to replace the HCB matrices representing each component of a system with an ensemble of random matrices, based on RMT. Each matrix in the ensemble must be close to the nominal matrix in the sense of some matrix norm and must meet certain requirements, such as symmetry and correct sign definiteness. However, the matrices are otherwise free and are not tied to any particular set of parameters in the FEM. Soize [ref. 6] used the maximum entropy principle to derive the positive definite and positive semidefinite ensembles SE^+ and SE^{+0} that follow the matrix variate gamma distribution and are capable of representing random structural matrices. This means the matrices in the ensembles are real, symmetric, and possess the appropriate sign definiteness to represent structural mass, stiffness, or damping matrices. As the dimension of the random matrix n increases, the matrix variate gamma distribution converges to a matrix variate Wishart distribution. In applications involving structural dynamics, the matrix dimensions are usually sufficient to give a negligible difference between the two distributions. Letting ensemble member random matrix G be any of the random mass, stiffness, or damping matrices, it is therefore assumed that G follows a matrix variate Wishart distribution, $G \sim W_n(p, \Sigma)$ in the remainder of this assessment.

In general, a Wishart distribution with parameters p and Σ can be thought of as the sum of the outer product of p independent random vectors S_i all having a multivariate normal distribution with zero mean and covariance matrix Σ. Parameter p is the number of random vectors used to

construct the matrices and is sometimes called the shape parameter. Using this approach, the random matrix G can be written as:

$$G = \sum_{i=1}^{p} S_i S_i^T \qquad S \sim N_n(0, \Sigma) \tag{1}$$

where the expected value is given by:

$$E(G) = \bar{G} = p\Sigma . \tag{2}$$

The dispersion or normalized standard deviation of the random matrix G is defined by the relation:

$$\delta_G^2 = \frac{E(\|G - \bar{G}\|_F^2)}{E(\|\bar{G}\|_F^2)} \tag{3}$$

in which $\|*\|_F^2$ is the Frobenius norm squared.[3] It can be shown that Eq. (3) reduces to the expression:

$$\delta_G^2 = \frac{1}{p}\left[1 + \frac{(tr(\bar{G}))^2}{tr(\bar{G}^T\bar{G})}\right] = \frac{1}{p}[1 + \gamma_G] \tag{4}$$

where $\gamma_G = \frac{(tr(\bar{G}))^2}{tr(\bar{G}^T\bar{G})}$. The uncertainty in the random matrix G is dictated by the shape parameter p, which is the number of inner products in Eq. (1). The larger the value of p, the smaller the dispersion δ_G, although Eq. (4) shows that a fixed value of p does not imply a fixed dispersion. Suppose G_1 and G_2 represent structural matrices (e.g., stiffness) from two different system components. There are often instances when it is desired to have the same amount of uncertainty in each of the substructures. Eq. (4) shows that if $p_1 = p_2 = p$, then the dispersion values are not the same in general, $\delta_{G_1}^2 \neq \delta_{G_2}^2$, unless $\gamma_1 = \gamma_2$. To have the shape parameters between two matrices G_1 and G_2 be equal, p_1 must be set equal to p_2 and eliminated between the two relations, yielding:

$$\delta_{G_2} = \delta_{G_1}\sqrt{\frac{1+\gamma_2}{1+\gamma_1}} . \tag{5}$$

This expression leads to the definition of a normalized dispersion that is a function of the shape parameter:

$$\delta_{G_n} = \frac{\delta_{G_1}}{\sqrt{1+\gamma_1}} = \frac{\delta_{G_2}}{\sqrt{1+\gamma_2}} = \frac{1}{\sqrt{p}} . \tag{6}$$

It is important to realize, however, that just because two components have the same normalized dispersion, this does not mean that they will have the same uncertainty relative to a specific metric used to quantify component uncertainty. This is primarily due to the nonlinear dependence of the metric on the level of uncertainty.

---

[3] $\|*\|_F^2 = trace(*^T*)$

In the random matrix method developed by Soize [refs. 6 and 7] (referred to as method 1 by Adhikari [ref. 8]), the Wishart parameters are selected as p and $\Sigma = G_o/p$ where G_o is the nominal value of G, and the mean of the distribution is given by Eq. (2) as $\bar{G} = p\Sigma = p(G_o/p) = G_o$. Therefore, method 1 preserves the nominal matrix as the mean of the ensemble. In general, the nominal matrix can be decomposed as:

$$G_o = LL^T .\tag{7}$$

In the case of a positive definite matrix, this would just be the Cholesky decomposition. When the nominal matrix is positive semidefinite, an alternative decomposition approach can be used, as discussed in Reference 1. Let $(n \times p)$ matrix X be given by:

$$X = \begin{bmatrix} X_1 & X_2 \cdots X_p \end{bmatrix}\tag{8}$$

in which X_i is an $(n \times 1)$ column vector containing standard random normal variables such that $X_i \sim N_n(0, I_n)$. Note that $p \geq n$ must be satisfied for G to be full rank. An ensemble member $G \sim W_n(p, G_o/p)$ can then be easily generated for MC analysis using the expression:

$$G = \frac{1}{p} L X X^T L^T .\tag{9}$$

It was noted by Adhikari [ref. 8] that method 1 does not maintain the inverse of the mean matrix as the mean of the inverse, where:

$$E(G^{-1}) \neq [E(G)]^{-1} = \bar{G}^{-1} .\tag{10}$$

In some cases, $E(G^{-1})$ and $[E(G)]^{-1}$ can be vastly different, which is clearly not physically realistic. Instead, Adhikari [ref. 8] proposed method 3[4], in which the Wishart parameters are selected as p and $\Sigma = G_o/\theta$ where:

$$\theta = \frac{1}{\delta_G^2}[1 + \gamma_G] - (n + 1) .\tag{11}$$

An ensemble member $G \sim W_n(p, G_o/\theta)$ can then be generated using the relation:

$$G = \frac{1}{\theta} L X X^T L^T .\tag{12}$$

In this case, the inverse of the mean matrix is preserved as the mean of the ensemble inverses, where the mean matrix is given by:

$$\bar{G} = p\Sigma = p(G_o/\theta) = \frac{p}{\theta} G_o .\tag{13}$$

Note that in method 3, the dispersion defined in Eq. (3) is calculated with respect to the method 3 mean given in Eq. (13), and Eqs. (5) and (6) also hold. Note that the only difference between method 1 and method 3 is the normalization of the matrix—in other words, the matrices differ by a scale factor.

Experience has shown that the nonparametric method tends to skew frequencies up, in the sense that the mean frequencies from the random matrix ensemble are higher than the nominal. This

---

[4] Adhikari changes method/criteria numbers depending on the reference. It is method 3 for the cited reference.

effect was minimized by choosing method 1 (i.e., matching the matrix mean) for the mass matrix and method 3 (i.e., matching the matrix inverse mean) for the stiffness matrix. Therefore, the nonparametric portion of the HPV method is based on a method-1 randomization of a component mass matrix and a method-3 randomization of the component stiffness matrix. In general, structural components can be weighed and mass center locations determined using computer software, so it is common practice in analytical model validation to assume that the error in a model is concentrated in the stiffness matrix rather than the mass matrix. Therefore, in this application, only the component stiffness matrices are randomized. The component mass matrices are assumed to have no uncertainty.

The Wishart matrix uncertainty model results in uncertainty in both frequencies and mode shapes. However, an extensive amount of MC simulation and analysis performed during this and previous assessments has shown that, in comparison to modal frequencies, the corresponding component mode shapes tend to be much more sensitive to the nonparametric matrix randomization provided by methods 1 and 3. Therefore, the HPV approach possesses a parametric component of uncertainty in which the eigenvalues of the FI modes in the component HCB representation are assumed to be random variables. The FI eigenvalues are then random parameters within the HCB component stiffness matrix. During each iteration within an MC analysis, a random draw of HCB FI eigenvalues is selected to generate a random HCB component stiffness matrix. Note that the mean of this ensemble would just be the nominal HCB stiffness matrix. However, for the current iteration, the parametrically randomized HCB stiffness is treated as the nominal matrix for NPV, and method 3 is applied to provide model-form uncertainty on top of the FI eigenvalue uncertainty. This is analogous to the approach proposed by Capiez-Lernout [ref. 9] for separating parametric and nonparametric uncertainty. In contrast to the nonparametric model-form uncertainty, the mode shapes are relatively insensitive to the parametric FI eigenvalue uncertainty. Therefore, the HPV approach provides the capability to almost independently adjust the uncertainty in the component frequencies and mode shapes. However, this characteristic is problem dependent and should be checked during each application.

The HPV method has the capability of preserving rigid-body motion and rigid-body mass properties. It can also preserve the certainty of subsets of component modes. For example, in previous assessments, the component slosh modes were assumed to have no uncertainty. Details on how to handle these special cases are presented in Reference 1.

5.1.1 Randomization of Component FI Eigenvalues using Gaussian Process Models

In past assessments [ref 1], the component FI eigenvalues were considered as independent random variables. It was shown in Section 5.6.4 of Reference 1 that even though the variation of the FI eigenvalues is parametric with respect to the HCB representation, if they are varied independently, then it results in nonparametric variation of the stiffness matrix in physical space. In contrast, if the FI eigenvalues are varied in unison, i.e., perfectly correlated, it produces a purely parametric variation of the component stiffness matrix in physical space. As a component stiffness matrix varies, it is common to see the corresponding eigenvalues vary in a correlated manner to some extent, especially when they are closely spaced. Therefore, reality is somewhere between treating the FI eigenvalues as totally independent and treating them as perfectly correlated.

In this assessment, Gaussian Process (GP) modeling [ref. 10] was used to represent the random space of component FI eigenvalues. This means that any finite ensemble of component FI eigenvalue realizations follow a multivariate normal distribution. The characteristics of the realizations are determined by the mean vector $\bar{\lambda}$ and covariance matrix Σ or covariance function $\Sigma(x, x')$. In general, the covariance matrix or function corresponding to the FI eigenvalues of a component is unknown. However, in this assessment, it was assumed that the covariance function can be defined based on Euclidean distance. This covariance model is shown to be robust with respect to discrepancies between assumptions and reality in [ref 10]. Therefore, if $Y(x)$ is a realization of the FI eigenvalues, the covariance function is defined as:

$$Cov\big(Y(x), Y(x')\big) = \Sigma(x, x') = exp(-\|x - x'\|^2) \tag{14}$$

where x and x' are two points in FI eigenvalue space. The covariance between $Y(x)$ and $Y(x')$ decays exponentially fast as the distance between x and x' increases. The covariance matrix Σ_n is then generated by evaluating $\Sigma(x_i, x_j)$ in Eq. (14) at all pairs of the n component FI eigenvalues.

It is apparent that the covariance matrix derived based on Eq. (14) corresponds to unit scale or variance. In practice, it is desired to have the variance of the FI eigenvalues be based on the difference between the FEM and test eigenvalues or frequencies from the component modal test. Suppose that $\Delta\lambda$ is a vector of root-mean-square (RMS) uncertainties assigned to the FI eigenvalues based on the component modal test correlation results. In the case of a Gaussian distribution, the RMS uncertainty is equivalent to the standard deviation. The FI eigenvalue covariance matrix with the proper variance is then given by:

$$\Sigma_{nv} = diag(\Delta\lambda) * \Sigma_n * diag(\Delta\lambda) \tag{15}$$

where $diag(\Delta\lambda)$ is a diagonal matrix. If the jth eigenvalue λ_j is not uncertain, then $\Delta\lambda_j = 0$ and the jth row and column of Σ_{nv} are null, meaning that Σ_{nv} is positive semi-definite. Within MATLAB®, the command:

$$Y = mvnrnd\big(\bar{\lambda}, \Sigma_{nv}, 1\big) \tag{16}$$

produces a finite realization of the random FI eigenvalues under a GP prior with a specific mean and covariance, which can be easily implemented within a MC analysis.

5.1.2 Mixed Boundary Approach for Assigning HCB Eigenvalue Dispersions

The HPV method for modeling component uncertainty used in this assessment requires the selection of dispersion values for the HCB component FI eigenvalues and stiffness matrices. Ideally, these dispersion values are selected for each component based on component modal test results and the corresponding test-analysis modal correlation metrics. Test-analysis frequency error is used to identify the HCB FI eigenvalue uncertainties. However, one of the biggest challenges in the propagation of component test-analysis frequency error into uncertainty in the HCB flight configuration FI eigenvalues is that the component test and flight configuration boundary conditions and/or hardware are almost never the same. Because of this, it is difficult to match test configuration modes with flight configuration FI modes. The boundary condition mismatch can be alleviated using a newly developed mixed-boundary approach. In general, the

HCB flight configuration FI modes will be over-constrained when compared to the test configuration modes. The HCB component stiffness matrix can be written as

$$K_{CB} = \begin{bmatrix} K_S & 0 \\ 0 & \lambda \end{bmatrix} = \begin{bmatrix} K_{cc} & K_{cb} & 0 \\ K_{bc} & K_{bb} & 0 \\ 0 & 0 & \lambda \end{bmatrix} \tag{17}$$

where K_S is the component physical stiffness matrix statically reduced to the interface or boundary degrees of freedom (DOF), and the boundary DOF have been divided into two subsets: the c-set contains all DOF that are free in the component test configuration, and the b-set contains the DOF that are constrained in the component test configuration. When the HCB flight configuration is constrained at the test configuration interface DOF (b-set), it produces the mass and stiffness matrices:

$$M_C = \begin{bmatrix} M_{cc} & M_{cq} \\ M_{qc} & M_{qq} \end{bmatrix} \qquad K_C = \begin{bmatrix} K_{cc} & 0 \\ 0 & \lambda \end{bmatrix} \tag{18}$$

with corresponding eigenvalues λ_C and mass normalized eigenvectors $\phi_C = \begin{bmatrix} \phi_{cc}^T & \phi_{cq}^T \end{bmatrix}^T$. These eigenvalues and eigenvectors are consistent with the boundary conditions of the test configuration modes used in the component test-analysis correlation. Error or uncertainty in the analytical test configuration eigenvalues can be more easily mapped into uncertainty $\Delta\lambda_C$ in the eigenvalues of the system in Eq. (18). The HCB representation of the component using λ_C and ϕ_C as FI modal properties has the stiffness matrix and corresponding displacement vector given by:

$$K_B = \begin{bmatrix} K_{Sb} & 0 \\ 0 & \lambda_C \end{bmatrix} \qquad u_B = \{x_b^T \quad q_C^T\}^T \tag{19}$$

where K_{Sb} is K_S statically reduced to the b-set, x_b is the physical displacement of the b-set, and q_C are the modal coordinates of the FI modes with the c-set free. The transformation between displacement vector u_B and the original HCB displacement vector u_{CB} is then given by:

$$u_{CB} = \begin{Bmatrix} x_c \\ x_b \\ q \end{Bmatrix} = \begin{bmatrix} \psi & \phi_{cc} \\ I & 0 \\ 0 & \phi_{cq} \end{bmatrix} \begin{Bmatrix} x_b \\ q_C \end{Bmatrix} = T u_B . \tag{20}$$

The relation between K_B and K_{CB} is then:

$$K_B = T^T K_{CB} T \tag{21}$$

The test configuration HCB FI eigenvalues λ_C can be randomized (λ_{Cr}) based upon the component test-analysis correlation results, and the uncertainty can then be propagated into the random flight configuration HCB component stiffness (K_{CBr}) using the expression:

$$K_{CBr} = T^{-T} K_{Br} T^{-1} = T^{-T} \begin{bmatrix} K_{Sb} & 0 \\ 0 & \lambda_{Cr} \end{bmatrix} T^{-1} . \tag{22}$$

5.2 Hurty/Craig-Bampton Components and Uncertainty Models for R3A Configuration

The IMT/MSO components used in UQ analysis were based on the R3A integrated FEM provided by MSFC Structural Dynamics & Integration Branch, except for the CS that was the FRAC version from IMT version R4. The FEM was divided into components and reduced to HCB representations for efficient MC UQ analysis. The following subsections describe the individual components and the identification of their associated uncertainty models. The frequency range of interest for the IMT was 0.0 to 7.0 Hz. Therefore, component FI modes were calculated to 15.0 Hz and augmented with residual vectors (RV) corresponding the component interfaces and the IMT shaker locations.

5.2.1 Mass Simulator for Orion – R3A Configuration

Due to possible scheduling conflicts and that the MPCV would add a multitude of complexities to the IMT, the MPCV was replaced by a mass simulator. The IMT R3A MSO and MSA, shown in Figure 5.2-1, were combined into a single FEM and reduced to an HCB component representation. The HCB component contains 152 DOF including 144 physical DOF at the interface between the MSA and the ICPS, and eight FI modal DOF. Only two of the FI modes have frequencies below 15.0 Hz. The component test/analysis correlation results for the updated MSO are listed in Table 5.2-1[5]. Note that the percentage modal frequency errors are computed relative to the FEM frequencies for UQ analysis. NASA Langley Research Center engineers stated that there were not enough sensors in the modal test to describe modes 10–14, therefore they were excluded in the formulation of the MSO/MSA uncertainty model. Based on the results in Table 5.2-1, the first MSO/MSA HCB FI mode at 6.33 Hz (1st bending along Y) was assigned an RMS frequency uncertainty of 3.91%, and the second MSO/MSA HCB FI mode at 6.34 Hz (i.e., 1st bending along Z) was assigned an RMS frequency uncertainty of 2.42%. The remaining six FI modes, corresponding to residual vectors (RV), were assigned a frequency uncertainty of 3.83%, which corresponds to the median frequency uncertainty in MSO FEM test configuration modes 3–9 listed in Table 5.2-1. During the process of combining the MSO and MSA FEMs, it was found that the MSO/MSA fixed-base modal frequencies could vary by as much as 10%, depending on just how the interface between the MSO and MSA was modeled. This additional uncertainty was addressed by adding an additional 10% frequency uncertainty to the uncertainties already assigned to the MSO/MSA FI frequencies based on the test results. This results in an eigenvalue uncertainty of 29.75% for FI mode 1, 26.38% for FI mode 2, and 29.57% for the other six FI modes.

---

[5] MSO Modal Test Correlation Summary, NASA LaRC, February 4, 2020.
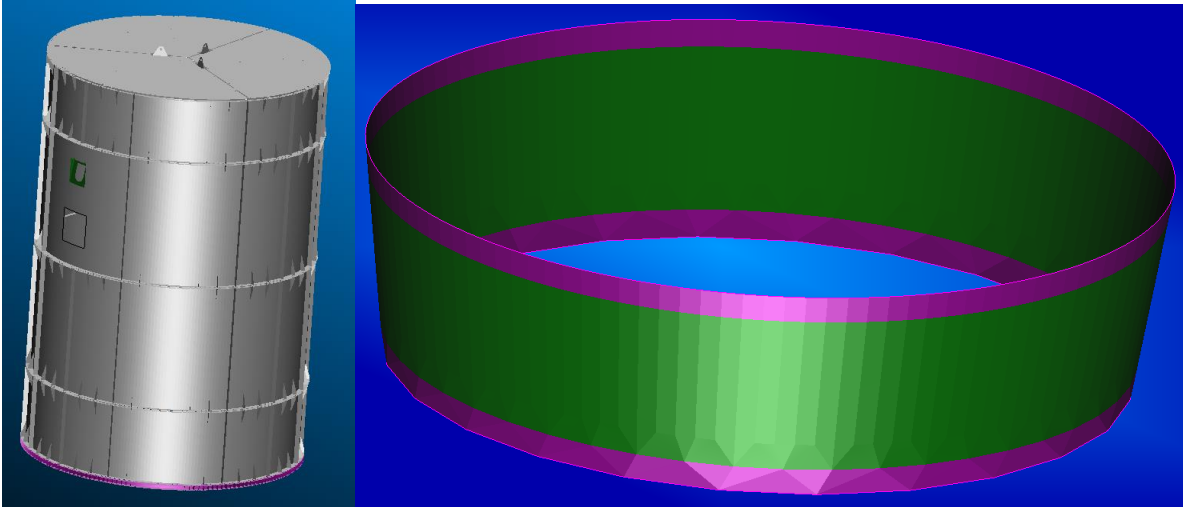
Figure 5.2-1. Computer Aided Design (CAD) Representations of MSO and MSA[6]

Table 5.2-1. Test/Analysis Correlation Results for Updated MSO

Mode	FEM Freq Hz	Test Freq Hz	% Error Freq	% Error Eigen	XO	Description
1	12.40	12.10	2.42	4.90	99	1st Bending Z
2	12.80	13.30	-3.91	-7.97	99	1st Bending Y
3	25.20	24.30	3.57	7.27	97	Top Oil Can
4	29.00	27.60	4.83	9.89	93	Tri-Lobe
5	29.70	28.80	3.03	6.15	89	Quad-Lobe
6	31.10	29.50	5.14	10.55	89	Tri-Lobe
7	31.30	30.10	3.83	7.81	95	Quad-Lobe
8	37.80	37.20	1.59	3.20	96	5-Lobe
9	40.00	37.90	5.25	10.78	96	5-Lobe
10	44.00	42.30	3.86	7.88	80	
11	45.50	43.40	4.62	9.44	72	
12	47.90	44.90	6.26	12.92	80	
13	49.60	47.00	5.24	10.76	92	
14	50.40	48.40	3.97	8.09	75	

Once the eigenvalue uncertainty is applied to the HCB stiffness matrix, the dispersion of the stiffness matrix is then applied using the NPV method discussed in Section 5.1. The dispersion level is determined based on the Diagonal Cross-Generalized Mass (DCGM) metric, which is the RMS value of the diagonal of the test/analysis XO matrix. Based on the XO results listed in Table 5.2-1, the value of DCGM for the MSO test over the first 9 modes is given by $\text{DCGM}_{Test} = 94.84$. A MC analysis was then performed in which the HCB stiffness matrix dispersion was selected and then 3,000 random MSO/MSA components were generated. The XO between the nominal and random HCB modes and the corresponding DCGM value were computed for each of the ensemble members for the first nine nominal modes, analogous to the test. The root-sum-square (RSS) XO [ref. 11] was computed as the XO for a linear combination of random modes within 3% of the frequency of the unique-best-fit mode. The most probable value of DCGM was then computed over the ensemble using a kernel density estimator and compared with the test value. The stiffness matrix dispersion was then adjusted, and the process

---

[6] Images taken from Flight Dynamic Risk Assessment (FDRA) Dry Run #3a (with MSO) Outbrief, May 28, 2020.

repeated, until the most probable DCGM value for the corresponding ensemble approximately matched the test value. More detailed descriptions of the process used to identify the stiffness matrix dispersion can be found in [ref 1]. For the MSO/MSA, a stiffness dispersion of $\delta_K = 21\%$ produced a most probable DCGM value of 94.96, which is comparable to the test value of 94.84. The corresponding normalized dispersion, defined in Eq. (6), has a value of $\delta_{Kn} = 3.11\%$. The relatively large value of the normalized stiffness dispersion indicates that the MSO/MSA component is not sensitive to model-form uncertainty. The average RMS frequency uncertainty over the nine HCB modes is 6.50%. Small differences between test-based and ensemble-based most probable DCGM values produce almost no change in predicted statistical results. Therefore, for simplicity, component stiffness matrix dispersions were limited to integer or half integer values.

5.2.2 Interim Cryogenic Propulsion Stage – R3A Configuration

The IMT R3A ICPS and LVSA, shown in Figure 5.2-2, were combined and the corresponding FEM was reduced to a single HCB component. The HCB representation contains 306 DOF including 288 physical DOF, 144 at the interface between the MSA and the ICPS, and 144 at the interface between the LVSA and the CS. There are 18 HCB FI modes, 12 of which are below 15.0 Hz. The remaining six are RVs. The IMT ICPS propellant tanks area is empty, so there are no slosh modes.
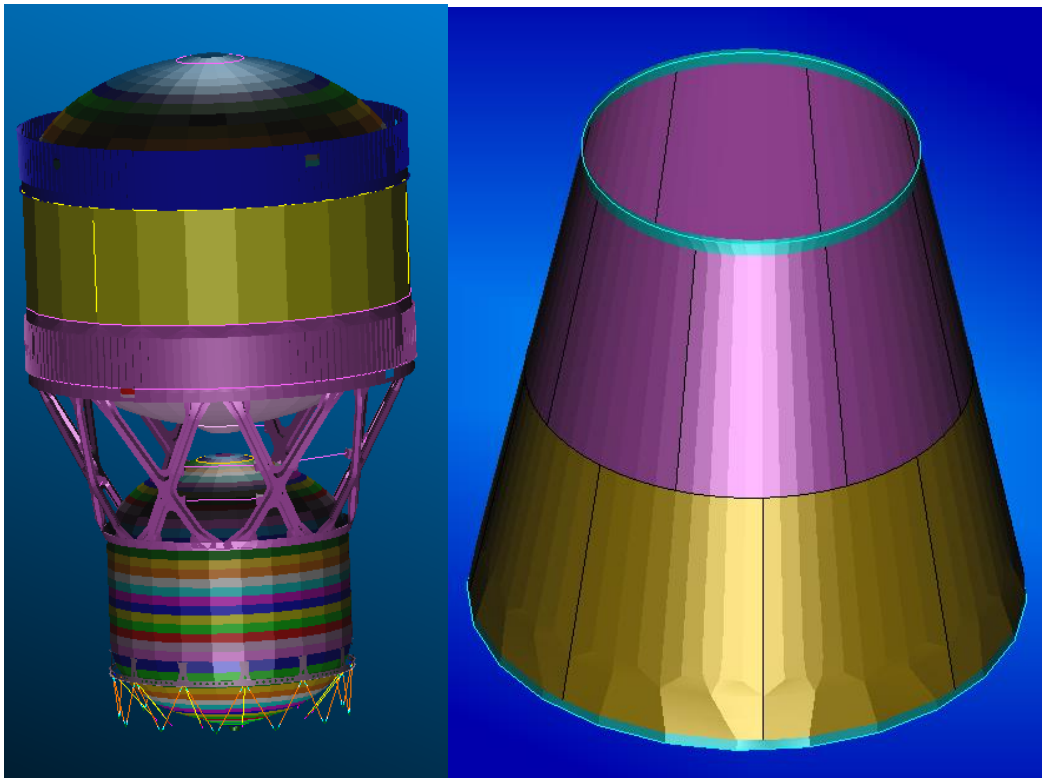
Figure 5.2-2. CAD Representations of ICPS and LVSA[7]

---

[7] Images taken from FDRA Dry Run #3a (with MSO) Outbrief, May 28, 2020.

Dispersion values for the updated ICPS/LVSA HCB component were based on the Integrated Spacecraft Payload Element (ISPE) configuration 3 modal test-analysis correlation results[8]. There were 11 FEM target modes matched to 11 of the 19 test modes. Only these target modes were considered in this analysis because the other eight modes were dominated by the MSA/MPCV simulator, which is not part of the ICPS/LVSA component. The test-analysis frequency correlation results are listed in Table 5.2-2.

Note that the ISPE was tested in a fixed-base configuration, while the ICPS/LVSA HCB FI modes are constrained at both the base, which is at the interface between the LVSA and the CS, and at the interface between the ICPS and the MSA. This mismatch in boundary conditions makes it difficult to match ISPE test configuration modes with the HCB FI modes to assign modal frequency uncertainty. Therefore, the mixed-boundary approach, discussed in Section 5.1.2, was used on the ICPS/LVSA HCB component. The DOF at the interface between the ICPS and the MSA were released during the component mode calculation, resulting in 162 fixed-base component modes that were compared with the fixed-base modes from the test configuration. However, there are still significant differences between the ICPS/LVSA flight article and the ISPE configuration 3 used in the test. For example, there was no fuel in the test article and the test article included the MSA, a CS simulator and an MPCV simulator. This makes it difficult to use frequency to match ICPS/LVSA fixed-base modes with ISPE test configuration modes. In many cases, test mode descriptions can be used to match modes, but this works best when the modes are low order and the descriptions are relatively simple. In the case of the ISPE, only three of the 11 target modes were easily described and probably insensitive to the hardware differences.

Table 5.2-2. Test-analysis Frequency Comparison for Configuration 3 Updated Model

FEM		Test				
Mode	Freq	Mode	Freq	% Error	XO	Description
5	16.61	2	17.06	-2.70	94	First bending
6	16.63	1	16.78	-0.89	95	First bending
7	18.38	3	18.12	1.43	95	LVSA shell ND 5
8	18.39	4	18.16	1.23	95	LVSA shell ND 5
9	19.55	5	18.78	3.96	97	LVSA shell ND 4
10	19.96	6	19.26	3.50	96	LVSA shell ND 4
13	20.90	10	21.02	-0.57	97	LVSA shell ND 6
14	20.91	9	20.96	-0.23	97	LVSA shell ND 6
19	25.81	15	25.90	-0.33	95	LVSA shell ND 7
20	25.81	14	25.82	-0.01	94	LVSA shell ND 7
24	31.01	19	32.47	-4.72	94	Second bending

Therefore, test-analysis frequency or eigenvalue error was mapped to the ICPS/LVSA fixed-base modes using MEM. The updated FEM ISPE configuration 3 MEM is dominated by the fundamental bending and, to a lesser extent, the second-order bending modes. The LVSA shell modes have little or no MEM. Table 5.2-3 lists the updated ISPE configuration 3 FEM modes matched to test modes sorted by uncertainty bin based on the MEM Euclidean norm, normalized to a maximum length of $\sqrt{6}$, and multiplied by 100.

---

[8] "ISPE Test/Analysis Model Correlation and Update, Modal and Static Test," Maasha, R., Fulcher, C., Lazor, D., Schmidt, A., Towner, R., Presentation to the NASA Joint Loads Task Team (JLTT), August 17, 2017.

Table 5.2-3. ISPE Updated FEM Configuration 3 MEM Magnitude by Bin

ISPE FEM Mode	MEM (%)	Freq. (Hz)	Description	Bin	% Freq. Dispersion	% Eigen. Dispersion
6	22.30	16.63	First bending	1	2.02	4.08
5	22.26	16.61	First bending	1	2.02	4.08
24	2.19	31.01	Second bending	2	4.72	9.66
20	0.02	25.81	LVSA shell ND 7	3	1.95	3.93
19	0.02	25.81	LVSA shell ND 7	3	1.95	3.93
8	0.01	18.39	LVSA shell ND 5	3	1.95	3.93
7	0.00	18.38	LVSA shell ND 5	3	1.95	3.93
9	0.00	19.55	LVSA shell ND 4	3	1.95	3.93
10	0.00	19.96	LVSA shell ND 4	3	1.95	3.93
14	0.00	20.91	LVSA shell ND 6	3	1.95	3.93
13	0.00	20.90	LVSA shell ND 6	3	1.95	3.93

Bin 1 was assigned a frequency dispersion of 2.02%, corresponding to the RMS error in the prediction of the first bending test mode pair. Bin 2 was assigned a frequency dispersion of 4.72%, corresponding to the test-analysis frequency error of the second-order bending test mode. The remaining LVSA shell test modes have little or no MEM. These modes define uncertainty Bin 3 with a frequency dispersion of 1.95%, corresponding to the RMS frequency error in the configuration 3 LVSA shell modes.

MEM was computed for the ICPS/MSA fixed-base modes. The first 22 modes up to 90.15 Hz account for approximately 99% of the effective mass over all six rigid body directions. Table 5.2-4 lists the first 30 ICPS/LVSA HCB fixed-base modes matched to the test configuration modes sorted by uncertainty bin based on the normalized MEM Euclidean norm. During the UQ analysis, the fixed-base mode uncertainty is mapped into the HCB FI mode uncertainty.

Based on the XO results listed in Table 5.2-2, the value of DCGM for the ISPE configuration 3 test over the 11 FEM/test mode pairs is given by $DCGM_{Test} = 95.44$. A MC analysis was performed in which the stiffness matrix dispersion was selected and then 3,000 random ICPS/LVSA components were generated. The 3% RSS XO between the nominal and random HCB modes and the corresponding DCGM value were computed for each of the ensemble members for the first 19 nominal modes with frequencies less than 15 Hz. The most probable value of DCGM was then computed over the ensemble and compared with the test value. The stiffness matrix dispersion was adjusted such that the most probable DCGM value for the corresponding ensemble matched the test value. For the ICPS/LVSA, a stiffness dispersion of $\delta_K = 15\%$ produced a most probable DCGM value of 95.06, which is close to the test value of 95.44. The corresponding normalized dispersion has a value of $\delta_{Kn} = 1.78\%$. The average RMS frequency uncertainty over the 19 HCB modes is 2.79%.

Table 5.2-4. ICPS/LVSA HCB Fixed-Base Sorted MEM Magnitude and Frequency Uncertainty by Bin

Bin	Number	Fixed-Base Mode	MEM	Freq. (Hz)	% Freq. Dispersion	% Eigen Dispersion
1	1	14	31.91	22.75	2.02	4.08
	2	22	27.29	90.15	2.02	4.08
	3	18	25.60	38.11	2.02	4.08
	4	13	24.52	22.07	2.02	4.08
	5	21	14.54	79.46	2.02	4.08
	6	15	12.51	25.57	2.02	4.08
	7	9	11.34	14.13	2.02	4.08
	8	6	10.18	12.60	2.02	4.08
2	9	19	6.68	44.48	4.72	9.66
	10	20	5.00	47.33	4.72	9.66
	11	5	3.98	11.17	4.72	9.66
	12	16	3.79	27.90	4.72	9.66
	13	10	3.69	14.32	4.72	9.66
	14	4	3.66	10.63	4.72	9.66
	15	3	1.21	4.96	4.72	9.66
	16	2	1.21	4.49	4.72	9.66
	17	7	1.13	12.96	4.72	9.66
	18	17	0.97	31.29	4.72	9.66
3	19	23	0.61	115.55	1.95	3.93
	20	25	0.51	123.35	1.95	3.93
	21	8	0.29	13.00	1.95	3.93
	22	1	0.17	3.11	1.95	3.93
	23	11	0.16	14.68	1.95	3.93
	24	24	0.05	122.86	1.95	3.93
	25	12	0.03	14.94	1.95	3.93
	26	30	0.01	132.45	1.95	3.93
	27	29	0.01	131.34	1.95	3.93
	28	35	0.00	155.33	1.95	3.93
	29	27	0.00	124.61	1.95	3.93
	30	26	0.00	124.05	1.95	3.93

5.2.3 FRAC Core Stage – R4 Configuration

The IMT R4 FRAC CS FEM, shown in Figure 5.2-3, was reduced to an HCB component with 224 DOF, including 168 physical DOF, 144 at the interface between the LVSA and the CS, and another 24 DOF at the interfaces between the CS and the solid rocket boosters (SRBs). There are 56 HCB FI modes, 50 of which are below 15.0 Hz. The remaining six are RVs. The IMT FRAC CS is empty, so there are no slosh modes, but CS pressurization stiffness is included corresponding to 4 psi. There are also 16 rigid body/mechanism modes and two very-low-frequency modes in the HCB representation. In the UQ analysis performed to determine the CS stiffness matrix dispersion, they were all treated as rigid body modes, meaning they had no uncertainty.
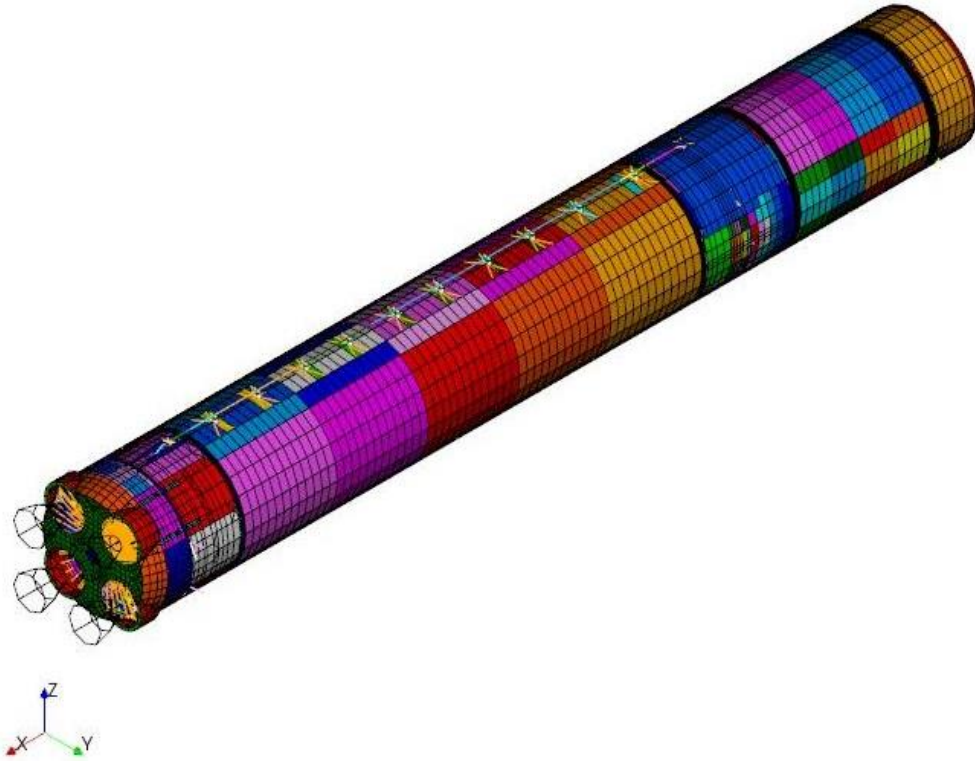
Figure 5.2-3. FRAC CS FEM

The FRAC CS test-analysis correlation results are shown in Table 5.2-5[9]. Eight test configuration FRAC CS modes were matched with eight test modes. The CS was tested in a simulated free-free configuration. Therefore, as in the case of the ICPS/LVSA, there is a mismatch between the test configuration boundary conditions and the boundary conditions applied to the CS HCB FI modes. Therefore, the mixed-boundary approach was also applied to the FRAC CS. To match the test configuration boundary conditions, all 168 HCB interface DOF were released, resulting in 224 free-free CS HCB modes that were compared with the CS test configuration modes. The eigenvalue dispersions of the HCB component modes were based on the test-analysis correlation results listed in Table 5.2-5. However, matching modes between the two sets to determine uncertainty could not be performed using MEM, as in the case of the ICPS/LVSA, because the modes are unconstrained, so they possess no MEM. Instead, the free-free CS HCB component modes were matched to the eight test configuration modes purely by the mode description listed in Table 5.2-5. The corresponding test-analysis eigenvalue error was then assigned to the HCB free-free component mode as the RMS eigenvalue uncertainty. The resulting eigenvalue uncertainties for the FRAC CS HCB free-free component modes are listed in Table 5.2-6. Note that there are 18 HCB modes matched to the eight test configuration modes because there are eight HCB engine pendulum modes and the HCB bending modes are not purely bending and instead are more complex bending mode pairs. In addition, to be conservative, all HCB modes matched to the 2nd bending mode about Z test configuration mode were given an eigenvalue uncertainty that is equal to the 8.65% uncertainty corresponding to the 2nd bending about Y test configuration mode instead of the 0% uncertainty listed in Table 5.2-5.

---

[9] FRAC_Model_Comparison_DTaMSS_303312020_Boeing - 3/31/2020
CS1 Model Validation and Model Assessments Plan – Integrated Analysis – Boeing – 5/21/2020

The remaining 188 elastic HCB free-free modes were assigned an eigenvalue dispersion of 6.27%, which corresponds to median eigenvalue uncertainty in the eight test configuration modes listed in Table 5.2-5. The median was used instead of the mean such that no one mode would have too much influence.

Table 5.2-5. CS Modal Test-Analysis Correlation Results

FRAC Freq Hz	CS Test Freq Hz	% FRAC Error Freq	% FRAC Error Eigen	XO Results	Description
5.18	5.33	-2.90	5.88	99	1st Bending MY
5.22	5.58	-6.90	14.27	98	1st Bending MZ
7.56	6.75	10.71	22.58	43	Engine Pendulum
7.94	7.68	3.27	6.66	79	1st Torsion
9.21	8.82	4.23	8.65	87	2nd Bending MY
9.38	9.38	0	0	89	2nd Bending MZ
11.29	11.34	-0.44	0.89	95	2nd Torsion
13.68	13.72	-0.29	0.59	89	Axial

Table 5.2-6. IMT FRAC CS HCB Free-Free Mode Eigenvalue Dispersions

HCB Mode	Freq	% Freq Dispersion	% Eigen Dispersion	Description
23	6.09	2.90	5.88	1st bending MY - pitch
24	6.63	6.90	14.27	1st bending MZ - yaw
25	6.85	2.90	5.88	1st bending MY - pitch
26	7.75	10.72	22.58	Engine pendulum
28	8.00	10.72	22.58	Engine pendulum
31	8.02	10.72	22.58	Engine pendulum
32	8.16	10.72	22.58	Engine pendulum
36	8.58	3.28	6.66	1st Torsion
45	9.55	10.72	22.58	Engine pendulum
46	9.59	10.72	22.58	Engine pendulum
47	9.59	10.72	22.58	Engine pendulum
48	9.60	10.72	22.58	Engine pendulum
57	12.08	0.44	0.89	2nd Torsional
67	15.44	0.29	0.59	1st axial
72	17.53	4.24	8.65	2nd bending MY - pitch
73	18.04	4.24	8.65	2nd bending MY - pitch
78	22.81	4.24	8.65	2nd bending MZ - yaw
79	22.88	4.24	8.65	2nd bending MZ - yaw

Based on the XO results listed in Table 5.2-5, the value of DCGM for the CS test over the seven FEM/test mode pairs, excluding the engine pendulum mode pair, is given by $\text{DCGM}_{Test} = 91.09$. The XO value for the engine pendulum mode was excluded because it was low compared with the other values, and not reflective of the overall quality of the test. MC analysis using 3,000 ensemble members and 3% RSS XO was performed to determine the HCB stiffness matrix dispersion that would provide a most probable DCGM value that agreed with the test value. The DCGM metric for each ensemble member was calculated over the 48 elastic modes with frequencies less than 15.0 Hz, excluding the two very-low-frequency modes mentioned earlier. For the IMT R3A FRAC CS HCB, a stiffness dispersion of $\delta_K = 8.5\%$ produced a most probable DCGM value of 91.03, which is comparable to the test value of 91.09.

The corresponding normalized dispersion has a value of $\delta_{Kn} = 0.88\%$. The average RMS frequency uncertainty over the 48 HCB modes is 4.70%.

5.2.4 Solid Rocket Boosters – R3A Configuration

The IMT R3A LSRB, shown in Figure 5.2-4, was reduced to an HCB component containing 98 DOF, including 48 physical DOF that interface to the CS, 44 FI modes with frequencies below 15.0 Hz, and six RVs. There was no specific modal test performed for the SLS SRBs. However, due to the SRB's heritage, the uncertainty models for the IMT 3A SRB HCB components were assumed to be at the updated level. It was also assumed that the SRBs have approximately the same level of test-analysis correlation, or uncertainty, as found in the updated ISPE, listed in Table 5.2-3. This means that the three HCB FI eigenvalue uncertainty bins are given by 4.08%, 9.66%, and 3.93%, and the HCB stiffness dispersion must be adjusted to produce a most probable DCGM value of 95.44 corresponding to the updated ISPE DCGM test value. In the case of the LSRB, the HCB FI eigenvalue and frequency uncertainty by bin are listed in Table 5.2-7 for the first 30 modes based on normalized MEM magnitude. A HCB stiffness dispersion of 2.5% produced a most probable DCGM value of 95.40 when computed using the 42 elastic HCB modes below 15.0 Hz, which compares well with the test value. The corresponding mean RMS frequency uncertainty is 1.94%.

Figure 5.2-4. CAD Representation of SRB[10]

Table 5.2-7. LSRB Updated HCB FI MEM Magnitude and Frequency Uncertainty by Bin

Bin	Number	FI Mode	MEM	Freq	% Dispersion Eigen	% Dispersion Freq
1	1	1	52.45	1.90	4.08	2.02
	2	2	42.14	2.07	4.08	2.02
	3	16	22.29	9.87	4.08	2.02
	4	15	11.05	9.27	9.66	2.02
2	5	49	4.26	21.95	9.66	4.72
	6	5	3.26	6.58	9.66	4.72
	7	50	3.02	22.23	9.66	4.72
	8	13	2.81	8.33	9.66	4.72
	9	47	2.72	19.87	9.66	4.72
	10	24	2.68	11.12	9.66	4.72
	11	46	2.18	19.70	9.66	4.72
	12	22	1.68	11.03	9.66	4.72
	13	48	1.67	21.43	9.66	4.72
3	14	4	0.95	5.47	9.66	1.95
	15	34	0.62	12.99	9.66	1.95

[10] Image taken from FDRA Dry Run #3a (with MSO) Outbrief, May 28, 2020.

16	3	0.61	4.94	3.93	1.95
17	35	0.43	13.12	3.93	1.95
18	44	0.43	14.89	3.93	1.95
19	20	0.38	10.75	3.93	1.95
20	23	0.37	11.03	3.93	1.95
21	25	0.32	11.14	3.93	1.95
22	45	0.29	16.40	3.93	1.95
23	38	0.23	13.45	3.93	1.95
24	36	0.18	13.32	3.93	1.95
25	40	0.12	14.06	3.93	1.95
26	37	0.09	13.42	3.93	1.95
27	17	0.07	10.53	3.93	1.95
28	30	0.06	12.09	3.93	1.95
29	39	0.06	14.01	3.93	1.95
30	12	0.05	7.87	3.93	1.95

The RSRB HCB component was assigned the same uncertainty model as the LSRB.

5.2.5 Mobile Launcher – R3A Configuration

The IMT R3A ML FEM, shown in Figure 5.2-5 was considered to have a pretest level of uncertainty. The FEM was constrained at the six VAB support posts and reduced to an HCB representation with 321 DOF, including 24 DOF that interface with other components, 286 FI modes to 15.0 Hz and 11 RVs. A modal survey of the ML only on the VAB support posts was performed at KSC on June 16–26, 2019. Test-analysis correlation results for the pretest ML are shown in Table 5.2-8 for 16 primary target modes[11].

There is a mismatch between the ML test configuration boundary conditions and those applied to the ML HCB FI modes. Therefore, the mixed-boundary approach was applied to the ML HCB to assign eigenvalue dispersions. The 24 HCB interface DOF were released during HCB mode computation, resulting in 321 fixed-base modes. Because the IMT R3A ML FEM and the pretest FEM used in the test-analysis correlation are equivalent, the HCB fixed-base modes were directly matched to the test configuration target modes listed in Table 5.2-8. The corresponding test configuration eigenvalue errors were assigned as dispersions to the corresponding HCB fixed-base modes. The remaining HCB fixed-base modes were assigned an eigenvalue dispersion of 21.52%, corresponding to the median eigenvalue error for the 16 target modes. Based on the XO values in Table 5.2-8, the test value of the DCGM metric over the 16 target modes is 78.71. After applying the HCB fixed-base eigenvalue dispersions, the HCB stiffness dispersion was adjusted to produce a most probable DCGM value equivalent to the test value $\text{DCGM}_{Test} = 78.71$. During the MC stiffness dispersion analysis, the DCGM metric was computed for each ensemble member for the first 49 elastic modes with frequencies less than 8.0 Hz. The frequency range was limited to 8.0 Hz because the large number (286) of ML modes below 15.0 Hz made it difficult to compare test and analysis DCGM metrics in a meaningful way. An HCB stiffness dispersion of 6% produced a most probable DCGM value of 78.32, which was comparable to the test value. The corresponding mean RMS frequency uncertainty was 13.80% over the 49 modes.

---

[11] "Independent Assessment of the Mobile Launcher (ML) Only Modal Test Pretest Analysis," NESC-SHB-16-01110 (ITAR) (5-9-19 NRB); and Mobile-Launcher-Only Modal Survey Test Support, NESC-CR-16-01110_NASA-CR-2019-220415_ITAR
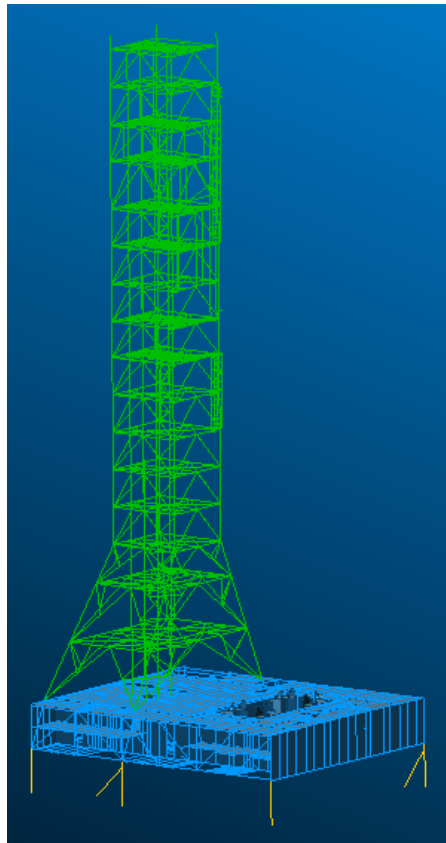
Figure 5.2-5. Pretest ML FEM on VAB Supports[12]

Table 5.2-8. Test-analysis Correlation Results for Pretest ML on VAB Support Posts

Test		FEM		% Error		
Mode	**Freq**	**Mode**	**Freq**	**Freq**	**Eigen**	**XO**
1	0.52	2	0.50	-3.95	-8.05	99
2	0.56	1	0.47	-19.53	-42.87	99
3	1.32	3	0.87	-51.34	-129.05	98
4	1.51	7	1.49	-1.64	-3.31	84
5	1.72	8	1.67	-3.18	-6.47	90
6	1.80	4	1.15	-56.40	-144.60	96
7	2.33	10	2.16	-7.98	-16.61	76
8	2.56	11	2.34	-9.52	-19.95	79
9	2.78	9	1.81	-53.59	-135.91	87
10	2.78	13	3.15	11.83	25.07	59
11	3.51	18	3.72	5.63	11.58	64
12	4.07	14	3.20	-27.33	-62.14	42
14	4.47	21	4.43	-1.01	-2.03	67
15	4.61	12	2.81	-63.85	-168.48	70
18	6.17	28	5.80	-6.43	-13.28	64
20	7.69	35	6.93	-10.94	-23.08	56

---

[12] Image taken from FDRA Dry Run #3a (with MSO) Outbrief, May 28, 2020.

5.3 IMT UQ Analysis for Uncertainty Model 1 – IMT-UM1

A UQ analysis was performed for the IMT configuration described in Sections 4.0 and 5.2 using MC analysis. An ensemble size of 10,015 random models was motivated by the use of order statistics to compute tolerance bounds for predicted results [ref. 12]. The goals of the analysis were to determine the amount of primary target mode frequency and shape uncertainty that could be expected during the actual IMT, and the probability that the selected shaker locations will excite the primary target modes using the selected sensor set. This assessment was completed prior to the IMT. However, during future posttest analysis, the test results can be compared to the UQ predictions. If the uncertainty predicted by the UQ analysis covers the test results, there is increased confidence that the HPV UQ method and the approach used to assign component uncertainty models presented in this report are valid.

The IMT reduced model contains 862 DOF and there are 70 modes below 7.0 Hz. Thirty-three target modes were originally selected during IMT R3A pretest analysis[13]. After discussions with MSFC, the list was reduced to 17 primary target modes, which were considered in this assessment. Table 5.3-1 lists the primary target modes with frequencies and partial mode descriptions.

Table 5.3-1. IMT R3A Primary Target Modes

No.	Mode	Freq (Hz)	Description
1	1	0.31	SLS Rocking ZX Plane
2	2	0.47	ML Tower 1st Bending XY Plane
3	3	0.50	ML Tower 1st Bending ZX Plane
4	4	0.52	SLS Rocking XY Plane
5	9	1.28	Core 1st Torsion
6	10	1.32	Core 1st Bending ZX Plane
7	11	1.53	
8	12	1.61	
9	13	1.62	SRB 1st Bending
10	14	1.70	
11	18	2.48	
12	19	2.64	
13	20	2.74	SLS Bounce (Trampoline)
14	23	3.14	Core Torsion + SRB Bending + MPCV Bending
15	24	3.20	Core Torsion + SRB Bending
16	35	4.78	SRB Torsion + Core Bending + MPCV Bending
17	36	4.81	SRB Torsion + Core Torsion

The component uncertainty models described in the previous section are summarized in Table 5.3-2. This system uncertainty model is designated as IMT-UM1.

Table 5.3-2. IMT-UM1

Component	Uncertainty Level	Assigned HCB FI Frequency Dispersion %	Stiffness Dispersion %	Normalized Stiffness Dispersion %
MSO	Updated	Modes: 3.91, 2.42; RVs: 3.83	21	3.11
ICPS/LVSA	Updated	3-Bins: 2.02, 4.72, 1.95	15	1.78
FRAC CS	Updated	Table 5.2-6	8.5	0.88
LSRB	Updated	3-Bins: 2.02, 4.72, 1.95	2.5	0.75
RSRB	Updated	3-Bins: 2.02, 4.72, 1.95	2.5	0.75
ML	Pretest	Table 5.2-8	6	1.78

---

[13] Files: IMT_MSO_Target.xml, ATA Engineering, Inc. and R3A_IMT_MSO_Compare.xlsx, MSFC

Based on the UQ analysis, the RMS uncertainty for the 17 target modes is illustrated in Figure 5.3-1. The greatest uncertainty, 23.06%, is in target mode 2, which corresponds to the ML tower 1st bending mode in the XY plane.
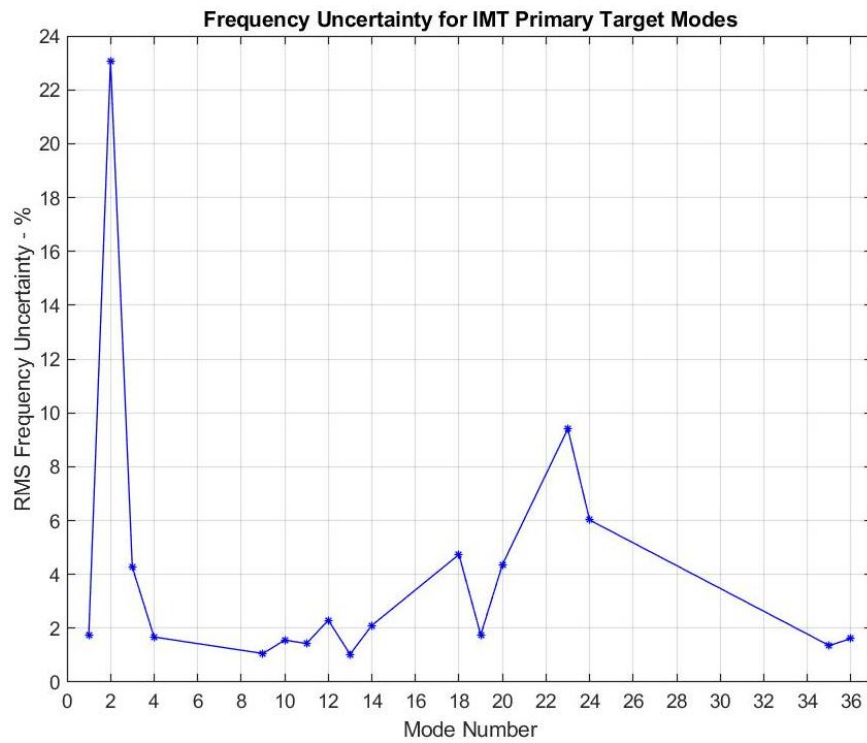

Figure 5.3-1. RMS Frequency Uncertainty for IMT Primary Target Modes – IMT-UM1

Figure 5.3-2 presents error bars for the target mode frequencies representing the range between the upper tolerance level at P99/90 and the lower tolerance level at P01/90. The corresponding interval provides an estimate of 98% enclosure with 90% confidence (P98/90). It can be seen that target modes 2, 18, 20, 23, and 24 possess the greatest frequency uncertainty. In all five of these modes, the ML possesses a significant amount of kinetic energy. Note that the nominal and median target mode frequencies are close in all 17 target modes. Figure 5.3-3 shows the IMT primary target mode RMS XO. Eleven of the target modes possess an RMS XO value greater than 0.90, while only one has a value less than 0.80. Uncertainty in target mode shapes can also be illustrated by estimating the probability density function for the DCGM metric, which is the RMS value of the diagonal of the nominal-random target mode XO for each of the 10,015 ensemble members. Figure 5.3-4 illustrates the estimated DCGM probability density function for the target modes. The most probable value is 92.45, while the mean and median values are 92.23 and 92.42, respectively. The P01/90 lower limit is 85.76. The modal parameter statistics presented in this report give a prediction of the amount of uncertainty that can be expected in the IMT. They can also be used to determine if the predicted uncertainty covers the IMT modal results, giving confidence in the HPV UQ procedure.
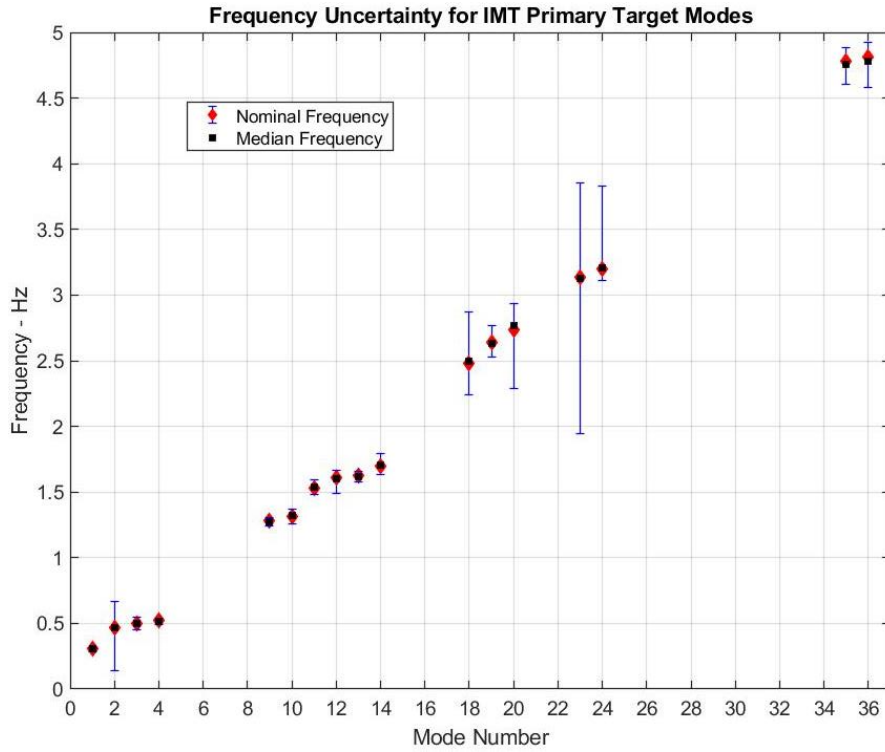
Figure 5.3-2. P98/90 Enclosure Intervals for IMT Primary Target Mode Frequencies – IMT-UM1
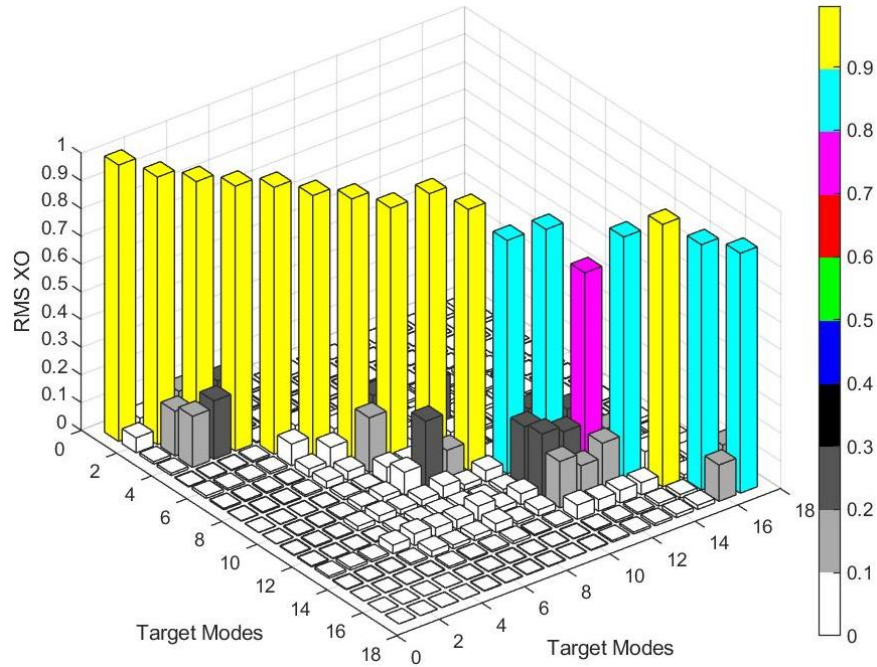

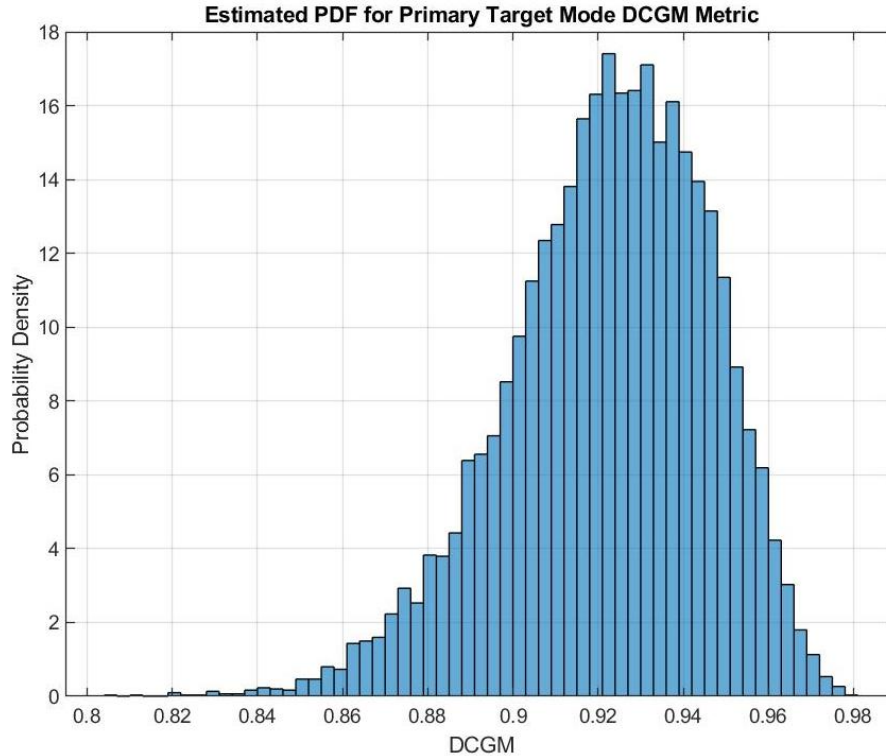*Figure 5.3-3. IMT Primary Target Mode RMS XO – IMT-UM1*

***Figure 5.3-4. Estimated Probability Density Function for IMT Primary Target Modes –
IMT-UM1***

Statistics were computed for acceleration frequency response and mode indicator functions for
the selected shaker and sensor configurations. A modal damping level of 1.0% and modes up to
16.0 Hz were included in the simulations. The shaker configuration selected for this assessment
is listed in Table 5.3-3. The IMT R3A sensor set containing 255 accelerometers is listed in
Appendix Table A-1. Figure 5.3-5 shows the XO between the nominal primary target modes and
the first 40 nominal IMT modes below 5.11 Hz, indicating that the target modes are nicely
decoupled from the other IMT modes using the R3A sensor configuration. A typical acceleration
frequency response at node 860 in the Y direction on the ICPS/LVSA due to input at shaker S36
is shown in Figure 5.3-6.

Table 5.3-3. Shaker Locations

	Shaker Label	**Node**	**Dir.**	**Location**
1	S50	3002573	X	ML Pad, Top Deck Surface Normal
2	S38	93579031	Y	ML Mid Tower
3	S51	3002292	Y	ML Pad, Top Deck Surface Parallel
4	S35	2812552	X	RSRB Surface Normal, -60 deg Off +Y on SRB Centerline (CL)
5	S36	650319	X	LH$_2$ Tank, +15 deg Off +Z Toward Core CL

The nominal and the P99/90 and P01/90 response levels are illustrated. During IMT posttest
analysis, the corresponding test result can be compared with the predicted uncertainty interval
shown in the figure. If the test result lies within the uncertainty interval, then confidence in the
validity of the HPV UQ method is enhanced.
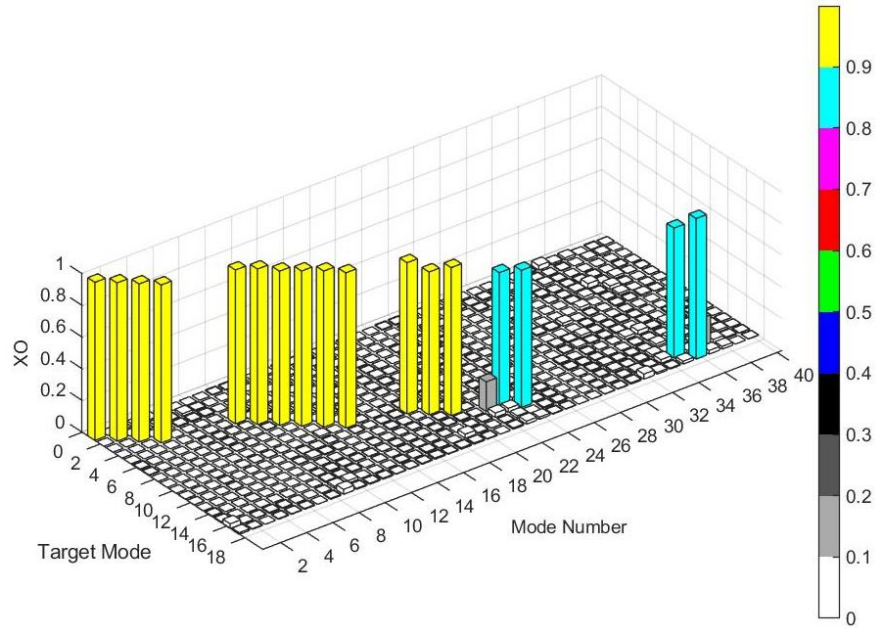
Figure 5.3-5. XO Between Target Modes and All IMT Modes Below 5.11 Hz
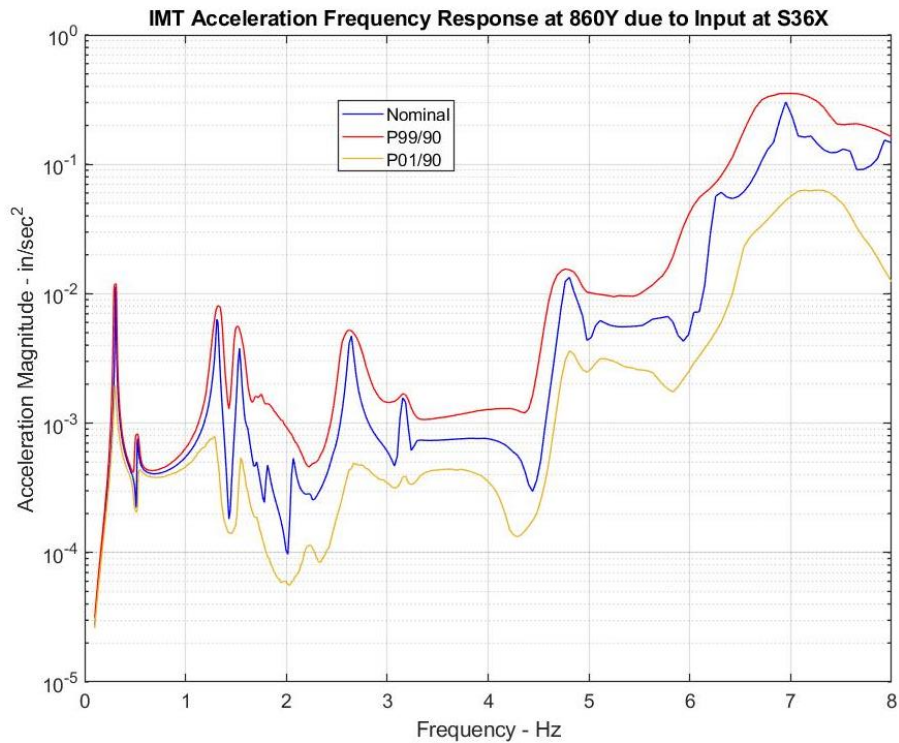
***Figure 5.3-6. Acceleration Frequency Response at 860Y due to Input from Shaker S36 –
IMT-UM1***

The CMIF gives a measure of how much the system is excited and responds using the designated shaker/sensor configuration. The CMIF plots the singular values of the frequency response matrix at each of the spectral lines. Peaks indicate the presence of excited modes. Figure 5.3-7 illustrates the CMIF corresponding to the maximum singular value as a function of frequency for the nominal system, and the P99/90 and P01/90 values. Figure 5.3-7 offers the advantage of

giving a measure of the overall response of the system over all sensors and shakers at once, instead of considering individual input-output relationships as illustrated in Figure 5.3-6. IMT CMIF results can be compared with Figure 5.3-7 to determine if the predicted uncertainty covers the test result.
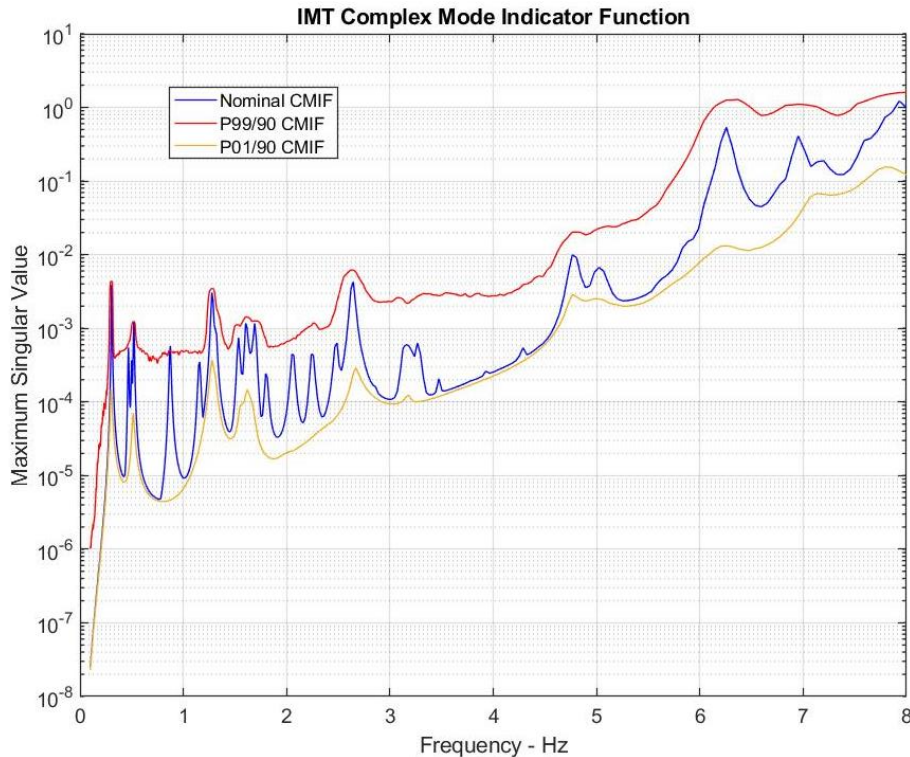
Figure 5.3-7. IMT CMIF – Maximum Singular Value of Frequency Response Matrix – IMT-UM1

The NMIF can be used to determine how effectively each of the primary target modes is excited and measured using the proposed shaker/sensor configuration. The NMIF is computed using the frequency response and is based on the fact that the real part becomes small near a resonance. One mode indicator function is computed versus frequency for each of the shakers, with values ranging between 0.0 and 1.0. A dip in an indicator function indicates the presence of a mode. In practice an NMIF value of 0.3 or smaller indicates that the mode is sufficiently excited and measured to be extracted from the test frequency response data. Therefore, for a mode to be sufficiently excited and measured, it must have an NMIF value less than or equal to 0.30 for any of the shakers. Figure 5.3-8 illustrates the minimum NMIF value over all shakers for each of the primary target modes for the nominal system. The values were determined by evaluating the NMIF functions at the nominal target mode frequencies. In practice, this approach is conservative because the minimum of the NMIF does not in general occur at the resonance, so this approach does not always capture the true minimum value. Using the criterion of NMIF being less than or equal to 0.30, 16 of the 17 primary IMT target modes are sufficiently excited and measured using the proposed shaker/sensor configuration. Figure 5.3-8 also shows the minimum P99/90 and P01/90 NMIF values for each target mode over all five shakers. The NMIF values corresponding to the random systems are determined by uniquely matching each of the nominal system target modes to a random mode and then evaluating the random NMIF function at the corresponding random resonant frequency. It can be seen from Figure 5.3-8, that there is a

significant amount of uncertainty in the NMIF values for all target modes. The median values of the target mode NMIF values over the ensemble are also presented in Figure 5.3-8. In many cases, the median NMIF values are close to the nominal values. Applying the 0.30 criterion to the median NMIF values, Figure 5.3-8 indicates that there is a 50% probability of identifying 15 of the 17 target modes during the IMT.
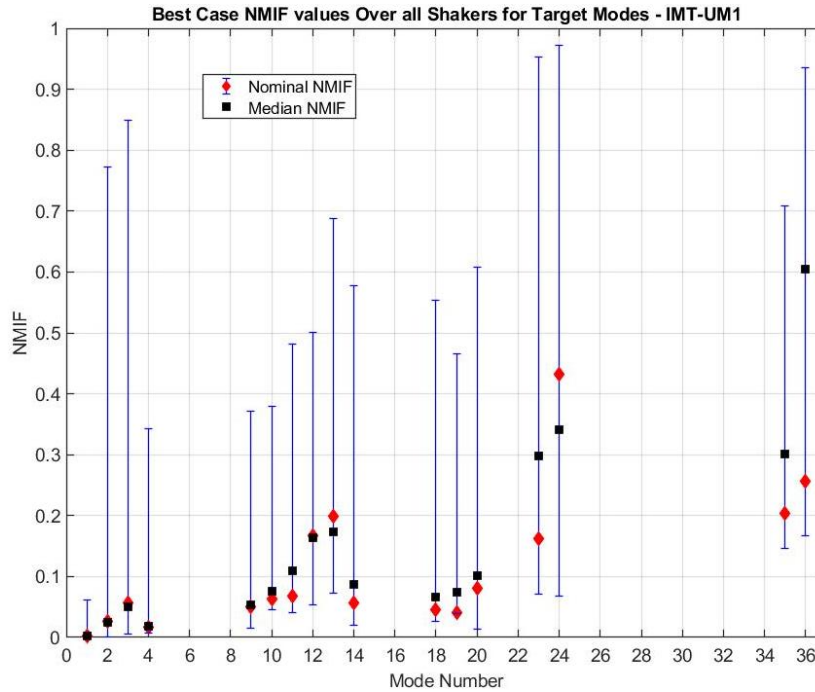
Figure 5.3-8. IMT Primary Target Mode NMIF Statistics – IMT-UM1

5.4 IMT UQ Analysis for Uncertainty Model 2 – IMT-UM2

At the time of this assessment, it was believed that the ML was the component with the greatest amount of uncertainty. However, as time goes on, the ML FEM is being continuously updated to better match test results. So, by the time that the IMT occurs, it is believed that the ML will have substantially less uncertainty than was assumed in the uncertainty model IMT-UM1 used in the previous section. To determine the impact of ML uncertainty and bracket the results, another UQ analysis was performed for the IMT R3A configuration in which the ML was assumed to have no uncertainty.

The system uncertainty model using the component uncertainty models described in the previous section, but with no uncertainty for the ML is designated as IMT-UM2 and summarized in Table 5.4-1.

Table 5.4-1. IMT Uncertainty Model 2 – IMT-UM2

Component	Uncertainty Level	Assigned HCB FI Frequency Dispersion %	Stiffness Dispersion %	Normalized Stiffness Dispersion %
MSO	Updated	Modes: 3.91, 2.42; RVs: 3.83	21	3.11
ICPS/LVSA	Updated	3-Bins: 2.02, 4.72, 1.95	15	1.78
FRAC CS	Updated	Table 5.2-6	8.5	0.88
LSRB	Updated	3-Bins: 2.02, 4.72, 1.95	2.5	0.75
RSRB	Updated	3-Bins: 2.02, 4.72, 1.95	2.5	0.75
ML	None	None	0	0.00

Based on the UQ analysis, the RMS uncertainty for the 17 primary target modes is illustrated in Figure 5.4-1 and compared with the uncertainty predicted using the previous uncertainty model IMT-UM1Figure 5.3-1. It is apparent that the uncertainty in the ML dominates the uncertainty in the IMT primary target mode frequencies. Without ML uncertainty, the maximum RMS frequency uncertainty is 1.11% in target mode 4, compared with a maximum of 23.06% in mode 2 when the ML has significant uncertainty.
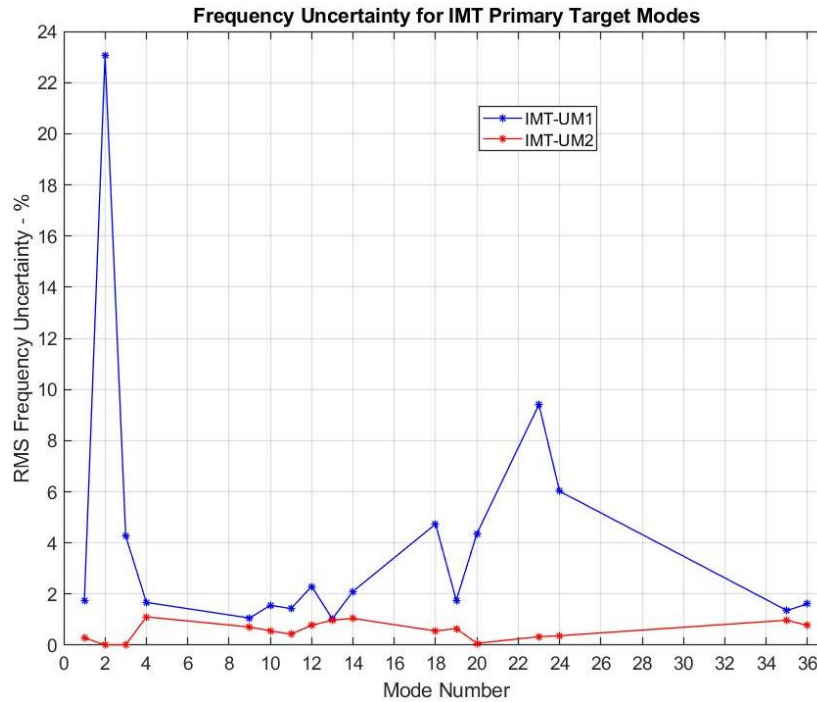

Figure 5.4-1. RMS Frequency Uncertainty for IMT Primary Target Modes – IMT-UM2

Figure 5.4-2 presents the P98/90 enclosure intervals for the IMT primary target mode frequencies in the case of no ML uncertainty. It can be seen that the confidence intervals are tight around the nominal frequencies for all of the target modes. Figure 5.4-3 shows the corresponding IMT primary target mode RMS XO. All 17 of the target modes possess an RMS XO value greater than 0.90, while only one of the off-diagonal terms is greater than 0.10. This indicates that the uncertainty in the target mode shapes is small when there is no ML uncertainty. Target mode shape uncertainty can also be illustrated by estimating the probability density function for the DCGM XO metric. Figure 5.4-4 shows the estimated DCGM probability density function for the target modes compared with the same result for the uncertain ML. When the ML has no uncertainty, it can be seen that the variance in the DCGM metric is much smaller. The most probable DCGM value is 99.74, while the mean and median values are 99.31 and 99.53, respectively. The distribution of the DCGM metric is more chi-square like, than normal. The corresponding P01/90 lower limit is 97.10. These results indicate that if the ML model continues to improve prior to the IMT, then the uncertainty in the IMT target modal parameters can be expected to be small. Figure 5.4-5 illustrates the P99/90 frequency uncertainty for the IMT primary target modes, while Figure 5.4-6 shows the corresponding P01/90 XO values for both ML uncertainty cases. If the IMT test-analysis correlation criteria for the target modes are frequency error less than or equal to 5.0% and an XO value greater than or equal to 0.90, then none of the target modes would pass the XO criterion at the P01/90 level and seven of the target

modes would pass the frequency criterion at the P99/90 level for the assumed uncertain ML. In the case where there is no ML uncertainty, 14 of the target modes would pass the XO criterion at the P01/90 level and all target modes would pass the frequency criterion at the P99/90 level.
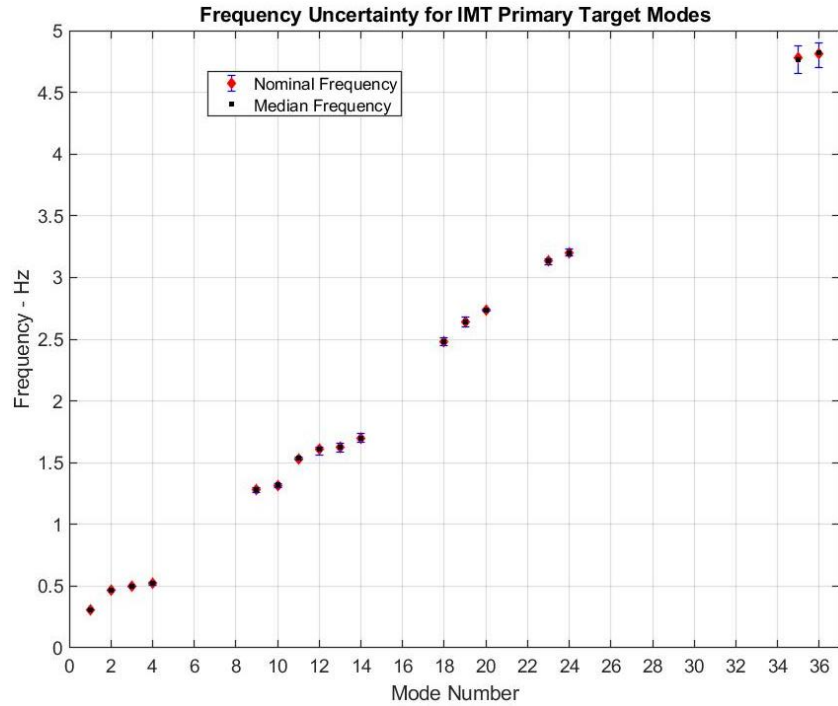
Figure 5.4-2. P98/90 Enclosure Intervals for IMT Primary Target Mode Frequencies – IMT-UM2
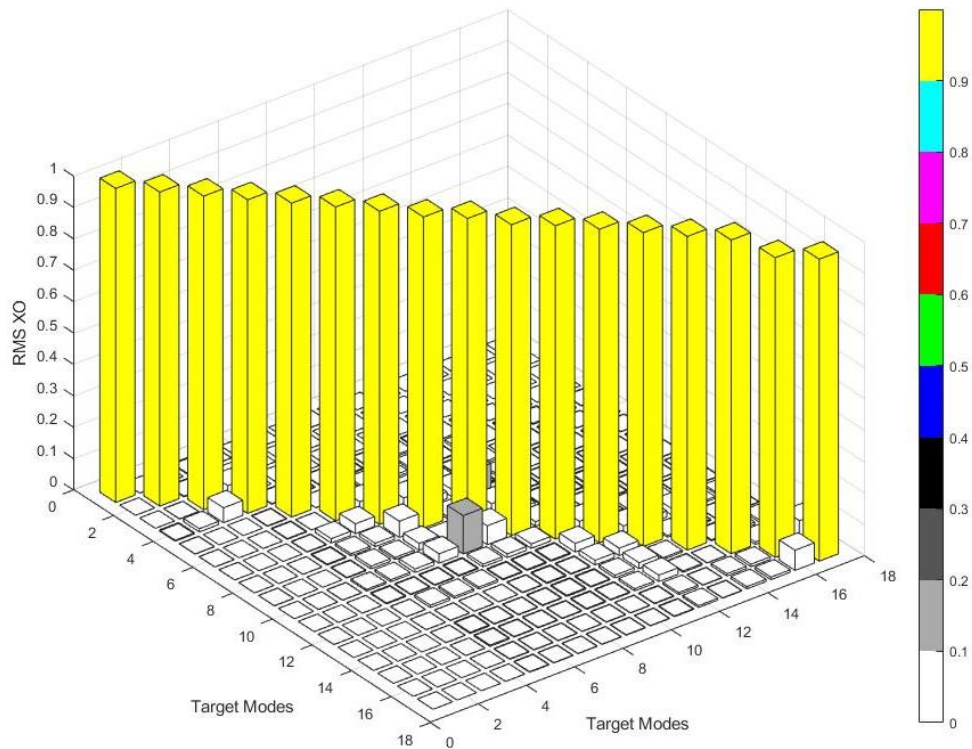
Figure 5.4-3. IMT Primary Target Mode RMS XO – IMT-UM2
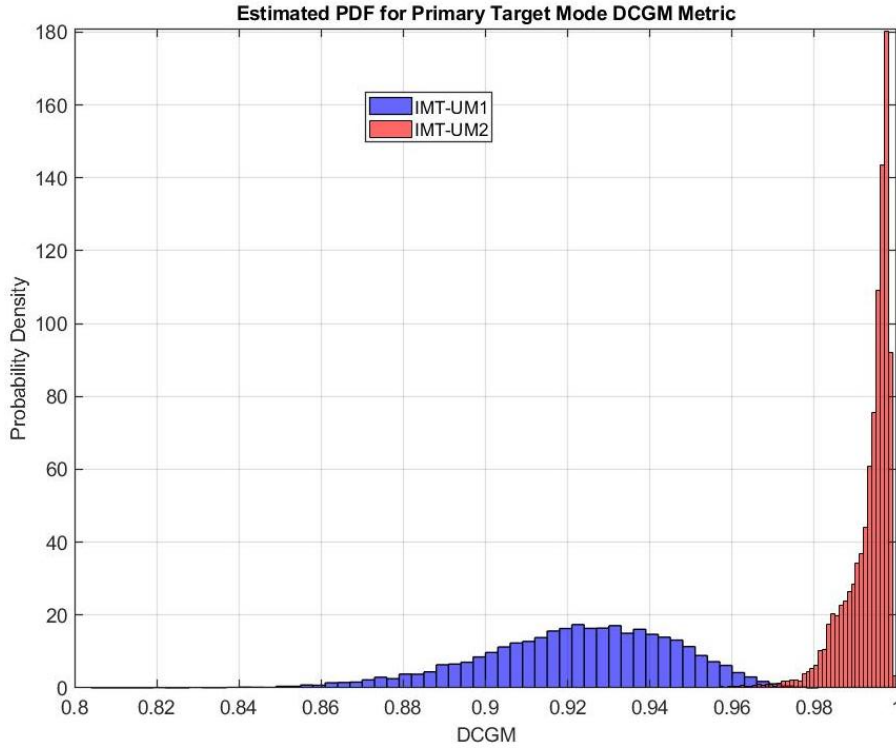
Figure 5.4-4. Estimated Probability Density Function for MT Primary Target Modes –
IMT-UM2
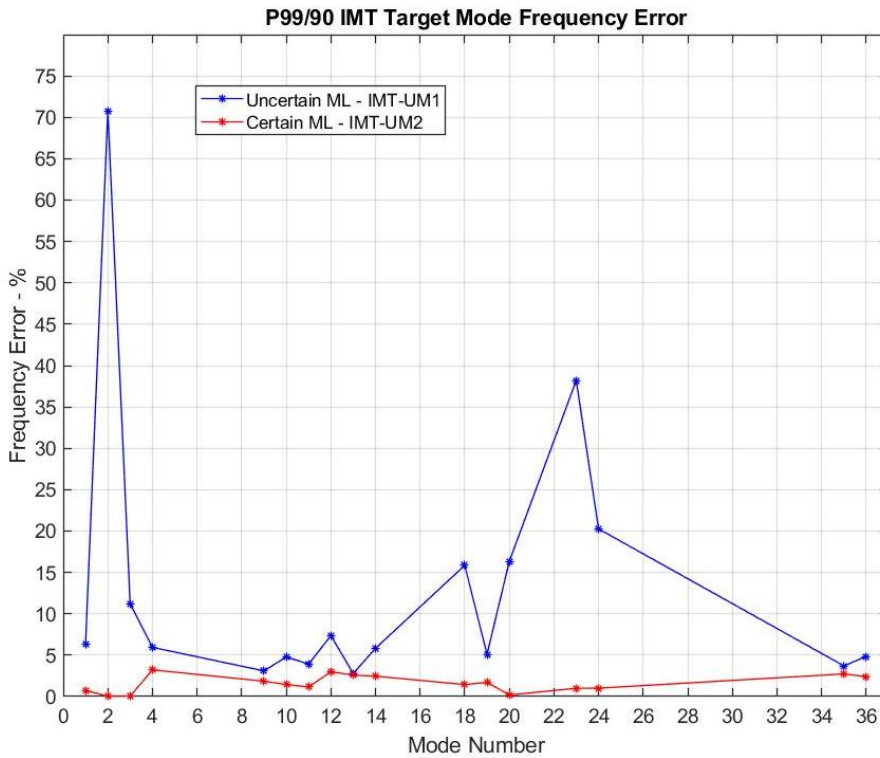
Figure 5.4-5. P99/90 IMT Target Mode Frequency Uncertainty
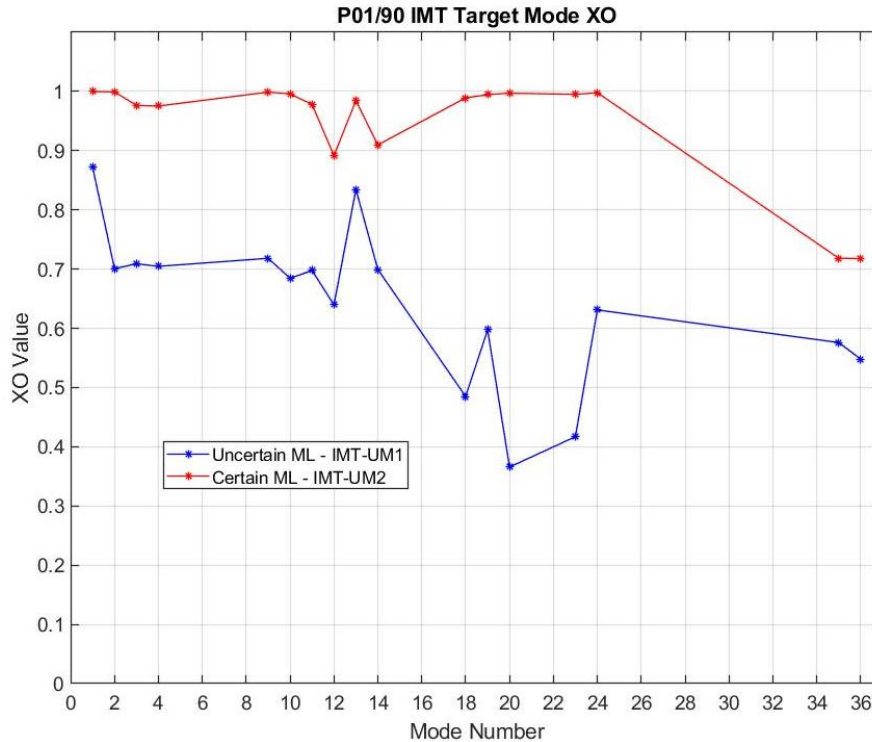
Figure 5.4-6. P01/90 IMT Target Mode XO

The tolerance limits for frequency and XO correlation illustrated in Figures 5.4-5 and 5.4-6 were determined using the method of order statistics. To do so, the conditions had to be considered separately. In practice, a target mode is said to be correlated if the frequency and XO correlation criteria are passed at the same time. Figure 5.4-7 shows the percentage of ensemble members that pass both correlation criteria for the certain and uncertain ML. In the case of the uncertain ML, two of the target modes are correlated in over 90% of the ensemble members, while in the case of no ML uncertainty, 15 of the target modes pass the correlation criteria in over 99% of the ensemble members.

As in the previous analysis, statistics were computed for acceleration frequency response and mode indicator functions for the selected shaker and sensor configurations. The acceleration frequency response at node 860 in the Y direction on the ICPS/LVSA due to input at shaker S36 is shown in Figure 5.4-8. The nominal and the P99/90 and P01/90 response levels are illustrated. Comparing the results for no ML uncertainty in Figure 5.4-8 with the uncertain ML response in Figure 5.3-6, it can be seen that the uncertainty in the frequency response between 1.2 and 3.2 Hz is significantly impacted by the ML uncertainty. Above 3.2 Hz, the uncertainty in the selected frequency response for the two cases is approximately the same.
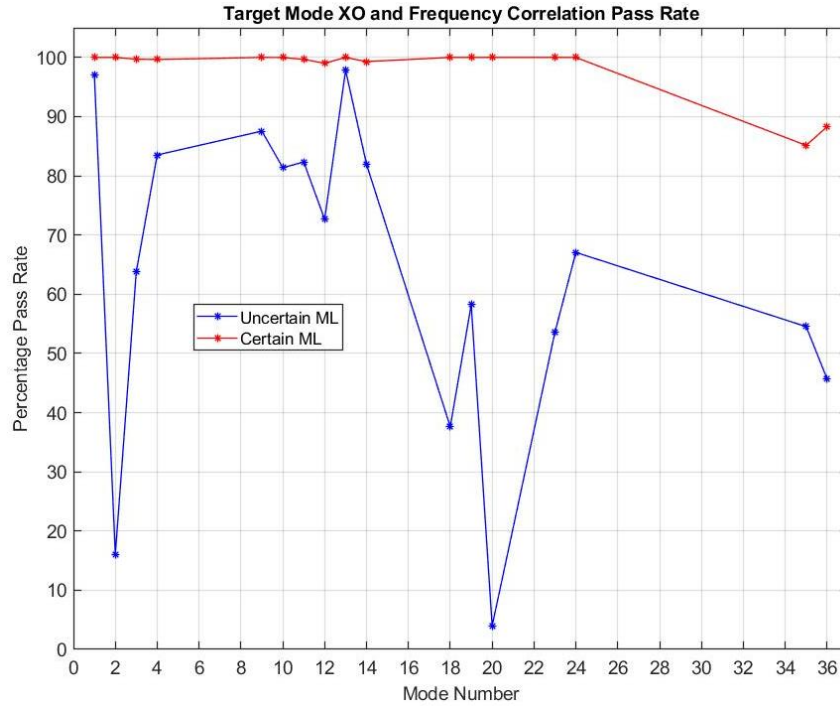
Figure 5.4-7. Percentage Pass Rates for Frequency and XO Correlation
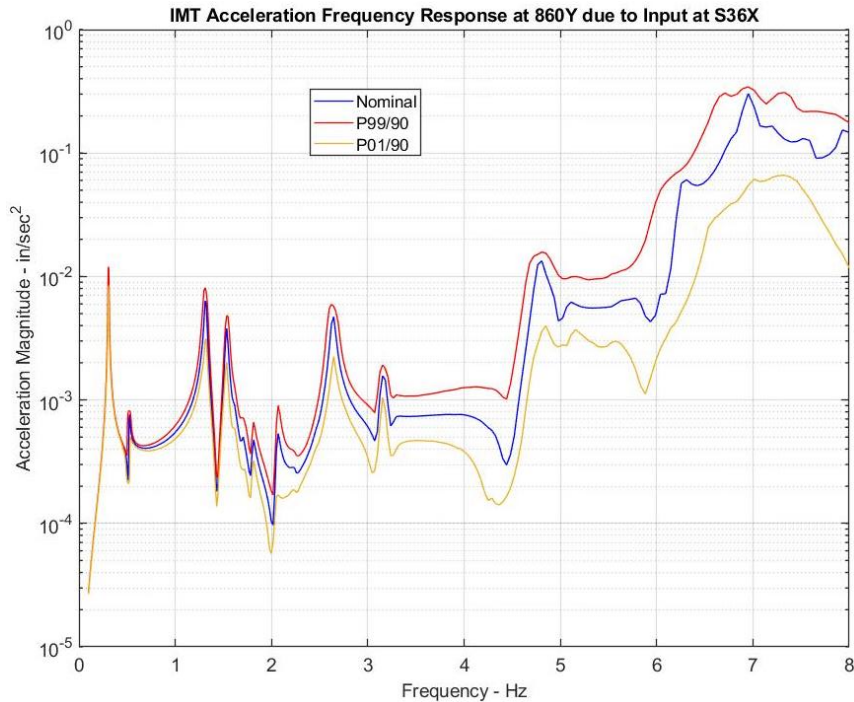
Figure 5.4-8. Acceleration Frequency Response at 860Y due to Input from Shaker S36 – IMT-UM2

The CMIF was also computed for the case of no ML uncertainty. Figure 5.4-9 illustrates the maximum singular value as a function of frequency for the nominal system, and the P99/90 and P01/90 values. Comparing these results with those in Figure 5.3-7 for the case of an uncertain ML, it can be seen that the ML uncertainty significantly impacts the uncertainty in the CMIF

maximum singular value at frequencies below 5 Hz. Figure 5.4-10 illustrates the minimum nominal NMIF values over all shakers for each of the primary target modes and also the minimum P99/90 and P01/90 NMIF values for each target mode over all shakers for the case without ML uncertainty. Comparing these results with those in Figure 5.3-8 for the case with ML uncertainty, several of the target mode NMIF values have significantly less uncertainty, while all NMIF values are less uncertain with no ML uncertainty. For the most part, the median NMIF values are lower when there is no ML uncertainty, as shown in Figure 5.4-11. These results indicate that as the uncertainty in the ML decreases, the probability of the target modes being accurately identified during the IMT increases.
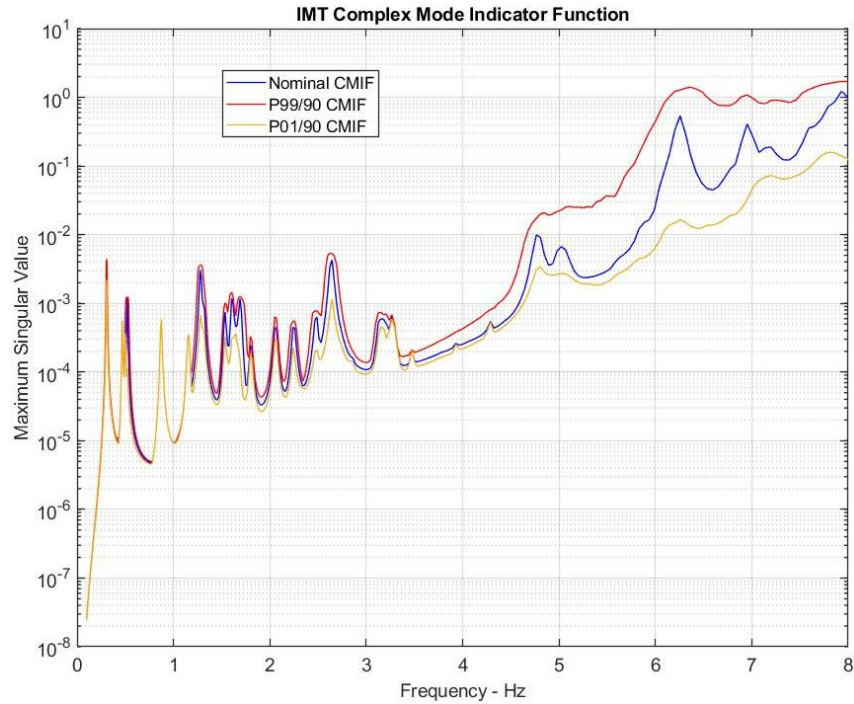
Figure 5.4-9. IMT CMIF – Maximum Singular Value of Frequency Response Matrix – IMT-UM2
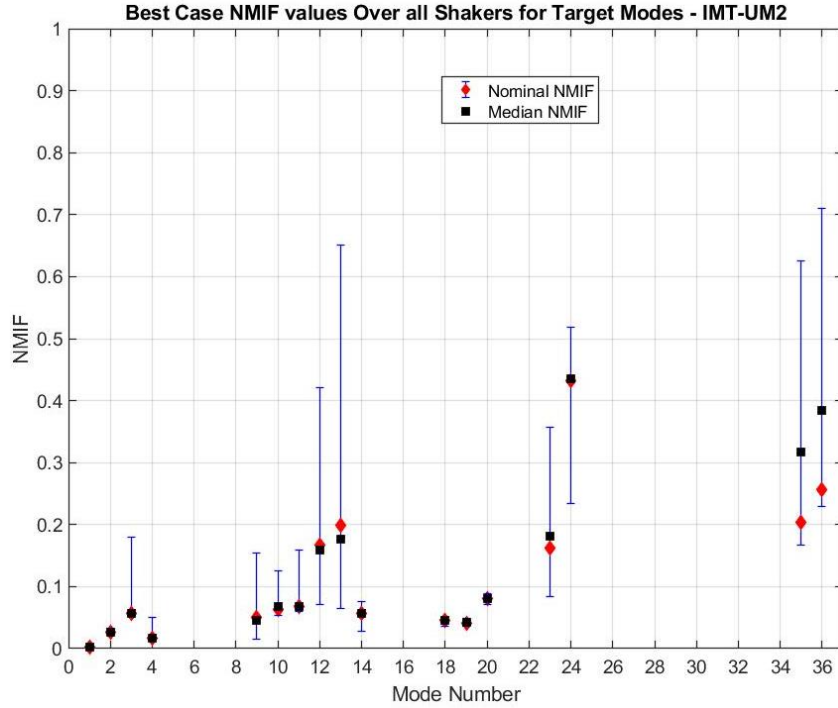
Figure 5.4-10. IMT Primary Target Mode NMIF Statistics – IMT-UM2
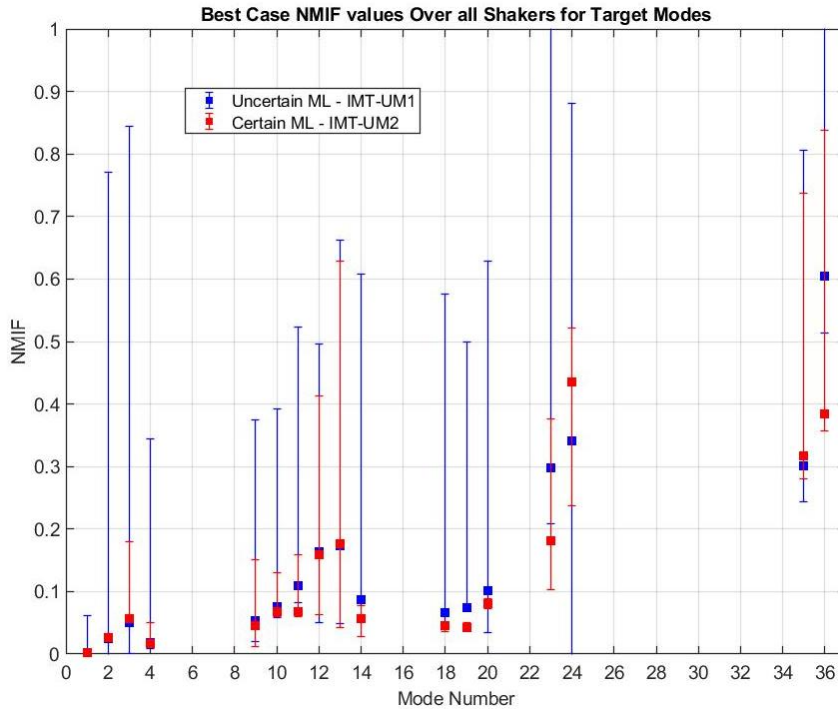
Figure 5.4-11. Target Mode Median NMIF and P98/90 Enclosure Intervals for UMs with and without ML Uncertainty

5.5 R4 IMT UQ Analysis for Uncertainty Model 3 – IMT-UM3

To be more consistent with future IMT test and analysis, a third UQ assessment was performed where the components were upgraded to the FRAC models that comprise the MSFC R4 IMT

configuration. Two shakers were added, the target mode set was changed to coincide with the latest R4 configuration, and the senor set was also updated. The FRAC ML component model was updated considerably over time based on component test results. Therefore, it was believed that while the results of this UQ analysis are not directly comparable to the results of the previous two UQ analyses, the uncertainty in the predicted results should lie somewhere between the uncertainties predicted for the IMT R3A configurations using the pretest VAC-1 ML in Section 5.3 and the certain ML in Section 5.4.

The IMT R4 reduced model contains 941 DOF and there are 70 modes to 7.18 Hz. Twenty-two primary target modes were selected for consideration in this UQ analysis. Table 5.5-1 lists the primary target modes with frequencies and partial mode descriptions.

Table 5.5-1. IMT R4 Primary Target Modes

No.	Mode	Freq (Hz)	Description
1	1	0.30	SLS Rocking XZ Plane
2	2	0.51	ML Tower 1st Bending XZ Plane
3	3	0.52	SLS 1st XY Bending
4	4	0.57	ML Tower 1st Bending XY Plane
5	6	1.26	Core 1st Torsion
6	7	1.30	SLS 1st XZ Bending
7	8	1.58	SLS 2nd XZ Bending
8	9	1.60	SLS 2nd XY Bending
9	10	1.62	SRB 1st Bending
10	11	1.72	SLS 3rd XY Bending
11	12	1.76	ML Tower Torsion
12	13	2.19	ML Tower 2nd XZ Bending
13	14	2.33	ML Tower/SLS 2nd XY Bending
14	15	2.54	ML Trampoline
15	16	2.59	CAA Vertical/SLS Bending
16	17	2.64	CAA Vertical/SLS Bending
17	18	2.88	CAA Vertical
18	19	2.95	ML Twisting/Tower Torsion
19	21	3.17	SLS 2nd Torsion
20	22	3.75	ML Tower Bounce/3rd Bending
21	23	4.00	ML Tower 3rd XZ Bending
22	27	4.63	SRB 2nd XY Bending/CAA lateral

The FRAC MSO/MSA HCB component has the same characteristics (i.e., number of aset DOF, number of FI modes below 15 Hz, etc.) as the R3A version described in Section 5.2.1. Due to model updates, the two fundamental bending FI modes increased in frequency to 6.44 Hz (i.e., 1st bending along Y) and 6.45 Hz (i.e., 1st bending along Z). The FI eigenvalue uncertainty that was assigned to the R3A MSO/MSA described in Section 5.2.1 was also applied to the FI eigenvalues in the R4 MSO/MSA HCB component. The HCB stiffness matrix dispersion analysis discussed in Section 5.2.1 was applied to the R4 MSO component and produced the same dispersion value of 21%.

As in the case of the MSO/MSA, the FRAC ICPS/LVSA HCB component also has the same characteristics as the R3A version described in Section 5.2.2. The modified-boundary approach

was applied to the HCB model and the MEM was calculated for the corresponding fixed-base modes, which was used to assign the modes to frequency bins based on the component test results listed in Table 5.5-2. This table lists the first thirty FRAC ICPS/LVSA HCB fixed-base modes matched to the test configuration modes sorted by uncertainty bin based on the normalized MEM Euclidean norm. The uncertainty bin assignments for R4 fixed-base modes are the same as those for the R3A version, but the modal frequencies differ slightly due to model updates. The HCB stiffness matrix dispersion analysis detailed in Section 5.2.2 was also applied to the FRAC ICPS/LVSA component. The resulting stiffness matrix dispersion was 15%, just as it was in the case of the R3A component. Therefore, the uncertainty model for the R4 ICPS/LVSA HCB component was identical to that assigned to the R3A version. The FRAC CS HCB component and uncertainty model are described in Section 5.2.3. The FRAC SRB HCB components and uncertainty models are also the same as the R3A versions. The components and uncertainty models are discussed in Section 5.2.4.

Table 5.5-2. FRAC ICPS/LVSA HCB Fixed-Base Sorted MEM Magnitude and Frequency Uncertainty by Bin

Bin	Number	Fixed-Base Mode	MEM	Freq. (Hz)	% Freq. Dispersion	% Eigen Dispersion
1	1	14	31.91	22.81	2.02	4.08
	2	22	27.29	90.75	2.02	4.08
	3	18	25.60	38.16	2.02	4.08
	4	13	24.52	22.10	2.02	4.08
	5	21	14.54	79.47	2.02	4.08
	6	15	12.51	25.58	2.02	4.08
	7	9	11.34	14.14	2.02	4.08
	8	6	10.18	12.60	2.02	4.08
2	9	19	6.68	44.57	4.72	9.66
	10	20	5.00	47.40	4.72	9.66
	11	5	3.98	11.17	4.72	9.66
	12	16	3.79	27.86	4.72	9.66
	13	10	3.69	14.32	4.72	9.66
	14	4	3.66	10.63	4.72	9.66
	15	3	1.21	4.96	4.72	9.66
	16	2	1.21	4.49	4.72	9.66
	17	7	1.13	12.96	4.72	9.66
	18	17	0.97	31.29	4.72	9.66
3	19	23	0.61	115.82	1.95	3.93
	20	25	0.51	123.47	1.95	3.93
	21	8	0.29	13.00	1.95	3.93
	22	1	0.17	3.11	1.95	3.93
	23	11	0.16	14.68	1.95	3.93
	24	24	0.05	122.87	1.95	3.93
	25	12	0.03	14.94	1.95	3.93
	26	30	0.01	132.50	1.95	3.93
	27	29	0.01	131.39	1.95	3.93
	28	35	0.00	155.44	1.95	3.93
	29	27	0.00	124.61	1.95	3.93
	30	26	0.00	124.06	1.95	3.93

The biggest change in the upgrade to the R4 IMT model was in the ML component. The version used in this UQ analysis was the MSFC ML modification delivered on August 28, 2020[14]. The

_____

[14] File: KSC-EMM-000001_SLS_ML1_MODAL_6pt_ShakerMod.dat

FEM was constrained at the six VAB support posts and reduced to an HCB representation with 401 DOF, including 24 DOF that interface with other components, 366 FI modes to 15.0 Hz and 11 RVs. A modal survey of the ML only on the VAB support posts was performed at KSC on June 16–26, 2019. Test-analysis correlation results for the FRAC ML are shown in Table 5.5-3 for 15 target modes (i.e., 14 primary and one secondary). The test frequencies and XO results were taken from Integrated Engineering Review Board presentation on ML1 FEM delivery to SLS[15].

Table 5.5-3. Test-analysis Correlation Results for FRAC ML on VAB Support Posts

Test		FEM		% Error		
Mode	Freq	Mode	Freq	Freq	Eigen	XO
1	0.52	1	0.52	0.30	0.60	98
2	0.56	2	0.57	1.97	3.97	100
3	1.32	3	1.07	-23.36	-52.19	95
4	1.49	4	1.54	3.30	6.72	98
5	1.71	5	1.72	0.49	0.99	92
6	1.80	6	1.75	-2.57	-5.21	94
7	2.33	7	2.26	-3.17	-6.43	95
8	2.56	8	2.55	-0.43	-0.87	95
9	2.77	9	2.80	1.24	2.50	86
10	2.83	10	2.94	3.59	7.32	98
11	3.52	11	3.43	-2.56	-5.20	93
12	4.03	12	4.00	-0.81	-1.64	82
13	4.15	13	4.09	-1.36	-2.74	88
14	4.43	14	4.59	3.39	6.89	70
16	5.76	21	5.72	-0.77	-1.55	57

Note that target mode three is a Crew Access Arm (CAA) mode that was in a different orientation during the modal test than what was modeled in the FRAC ML, therefore producing the large frequency error listed. For that reason, ML mode three was eliminated from the target mode set during the derivation of the FRAC ML uncertainty model.

There is a mismatch between the ML test configuration boundary conditions and those applied to the ML HCB FI modes. Therefore, the mixed-boundary approach was also applied to the FRAC ML HCB to assign eigenvalue dispersions. The 24 HCB interface DOF were released during HCB mode computation, resulting in 401 fixed-base modes. The HCB fixed-base modes were directly matched to the test configuration target modes listed in Table 5.5-3 using MEM and mode descriptions. The corresponding test configuration eigenvalue errors were assigned as dispersions to the corresponding HCB fixed-base modes. The remaining HCB fixed-base modes were assigned an eigenvalue dispersion of 3.35%, corresponding to the median eigenvalue error for the 14 target modes remaining after mode three was removed. Based on the XO values in Table 5.5-3, the test value of the DCGM metric over the 14 target modes is 89.77. After applying the HCB fixed-base eigenvalue dispersions, the HCB stiffness dispersion was adjusted to produce a most probable DCGM value equivalent to the test value, $DCGM_{Test} = 89.77$. During the MC stiffness dispersion analysis, the DCGM metric was computed for each ensemble

---

[15] File: 8-20-2020 IERB 3314 Approval_ML1_FEM_Delivery_to_SLS_Brown.pptx

member for the first 44 elastic modes with frequencies less than 8.0 Hz. The frequency range was limited to 8.0 Hz because there were 367 FRAC ML modes below 15.0 Hz, and the test DCGM metric was based on only 14 test modes. The greater the disparity between the number of test modes and component modes, the less meaningful the comparison between test and most probable DCGM metrics. An HCB stiffness dispersion of 4% produced a most probable DCGM value of 90.58, which was comparable to the test value. The corresponding mean RMS frequency uncertainty was 2.25% over the 44 modes. In comparison with the pretest ML discussed in Section 5.2.5, there is significantly less uncertainty in the R4 FRAC ML HCB component.

The R4 HCB component uncertainty models are summarized in Table 5.5-4. This system uncertainty model is designated as IMT-UM3. Based on the UQ analysis, the RMS uncertainty for the 22 target modes is illustrated in Figure 5.5-1. The greatest uncertainty of 3.23% is in mode 19, which corresponds to the ML twisting/tower torsion mode. Figure 5.5-2 presents the P98/90 enclosure intervals for the R4 primary target mode frequencies. It can be seen that all modes possess a small amount of frequency uncertainty. The nominal and median target mode frequencies are close in all 22 target modes. Figure 5.5-3 shows the IMT R4 primary target mode RMS XO. Twenty of the target modes possess an RMS XO value greater than 0.90, while two have values between 0.80 and 0.90. Note that no RSS analysis was performed to compute the XO values in this case. Uncertainty in target mode shapes can also be illustrated by estimating the probability density function for the DCGM metric, which is the RMS value of the diagonal of the nominal-random target mode XO for each of the 10,015 ensemble members. Figure 5.5-4 illustrates the estimated DCGM probability density function for the target modes. The most probable value is 96.10, while the mean and median values are 95.63 and 95.78, respectively.

Table 5.5-4. IMT-UM3

Component	Uncertainty Level	Assigned HCB FI Frequency Dispersion %	Stiffness Dispersion %	Normalized Stiffness Dispersion %
MSO	Updated	Modes: 3.91, 2.42; RVs: 3.83	21	3.11
ICPS/LVSA	Updated	3-Bins: 2.02, 4.72, 1.95	15	1.78
FRAC CS	Updated	Table 5.2-6	8.5	0.88
LSRB	Updated	3-Bins: 2.02, 4.72, 1.95	2.5	0.75
RSRB	Updated	3-Bins: 2.02, 4.72, 1.95	2.5	0.75
ML	Updated	Table 5.5-3	4	1.16
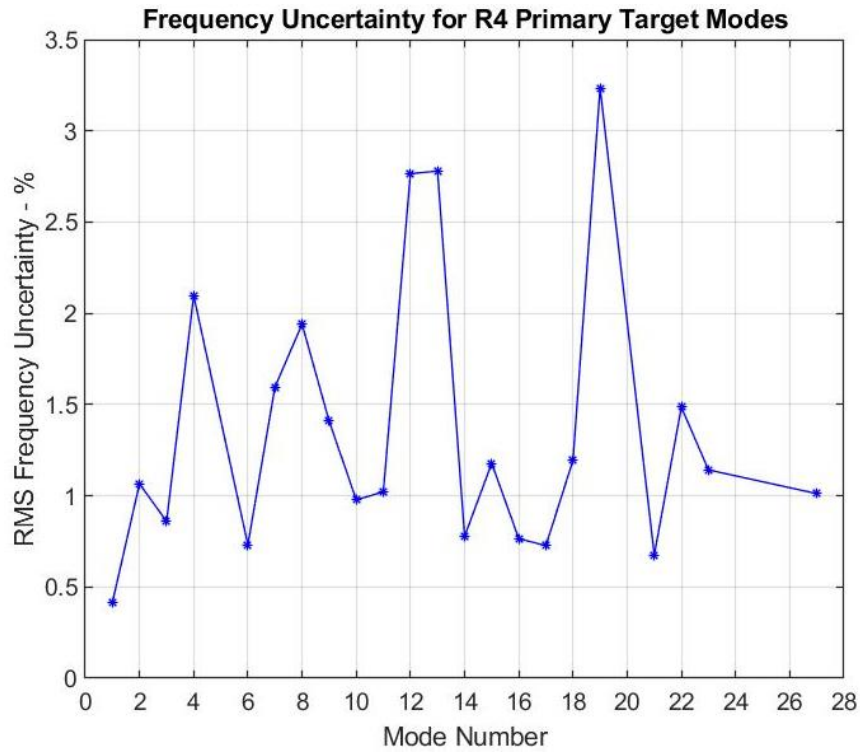
Figure 5.5-1. RMS Frequency Uncertainty for IMT R4 Primary Target Modes – IMT-UM3
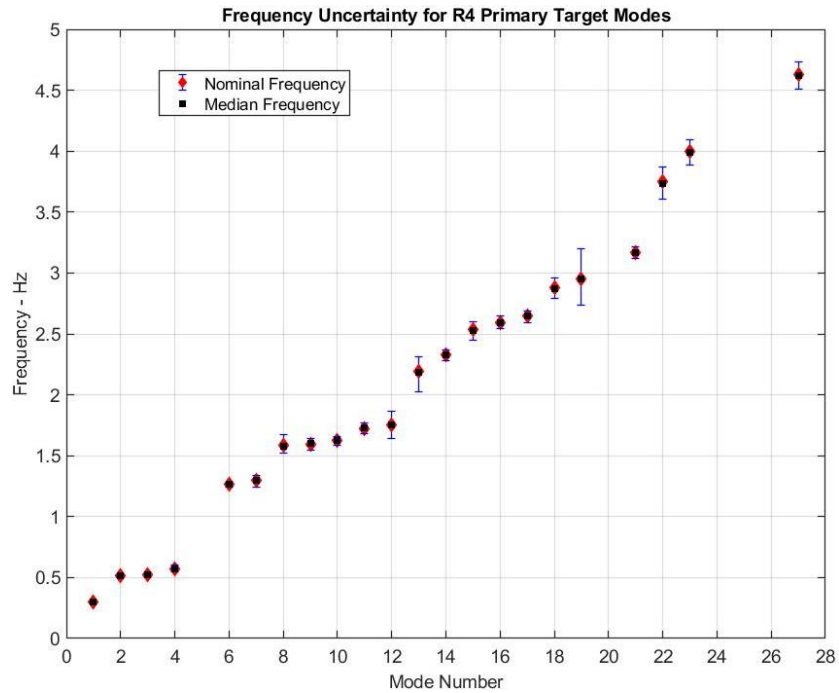
Figure 5.5-2. P98/90 Enclosure Intervals for IMT R4 Primary Target Mode Frequencies – IMT-UM3
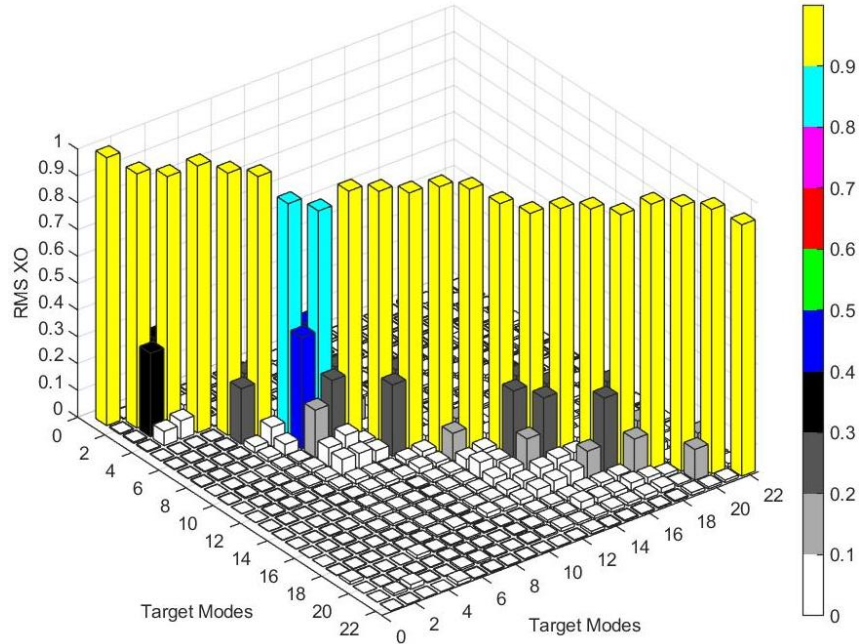
Figure 5.5-3. IMT R4 Primary Target Mode RMS Cross-Orthogonality – IMT-UM3
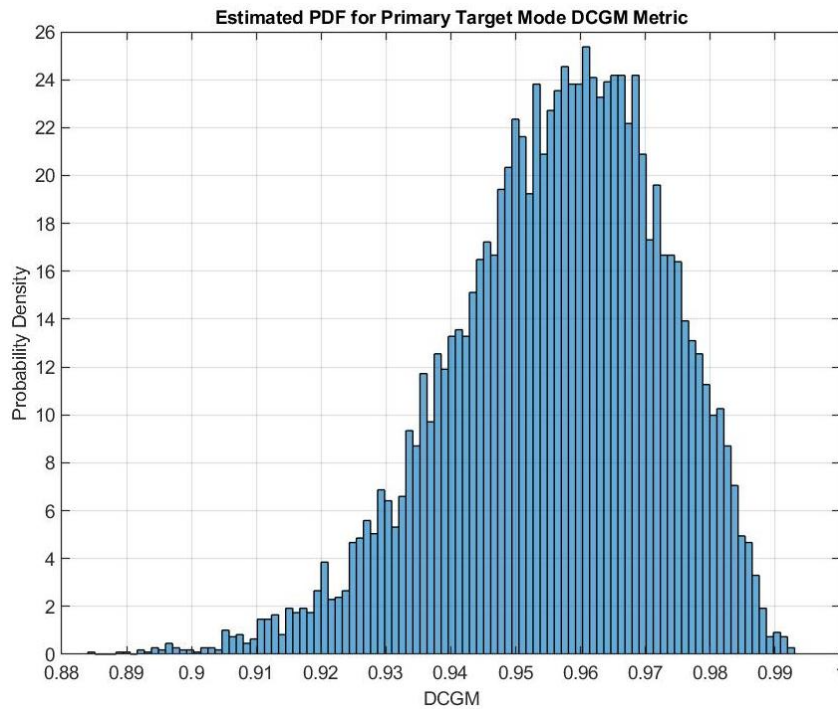
Figure 5.5-4. Estimated Probability Density Function for IMT R4 Primary Target Modes – IMT-UM3

The P01/90 lower limit is 91.12. Comparing the uncertainty predicted for the R4 IMT with that presented in Sections 5.3 and 5.4 shows that the FRAC ML model produces less uncertainty in the target modal parameters than the pretest ML model, but more uncertainty than the certain ML.

The IMT R4 sensor set contains 195 accelerometers as listed in Appendix Table A-2. Note that 143 of these sensors overlap with the R3A set listed in Appendix Table A-1. Figure 5.5-5 shows the XO between the nominal primary target modes and the nominal R4 IMT modes below 5.46 Hz with unobservable modes 20, 24, and 32 removed. The XO was computed using the R4 test analysis model (TAM) with the modes mass normalized with respect to the TAM mass. The largest off-diagonal value of 0.036 indicates that the target modes are nicely decoupled from the other observable IMT modes using the R4 sensor configuration and TAM mass matrix.
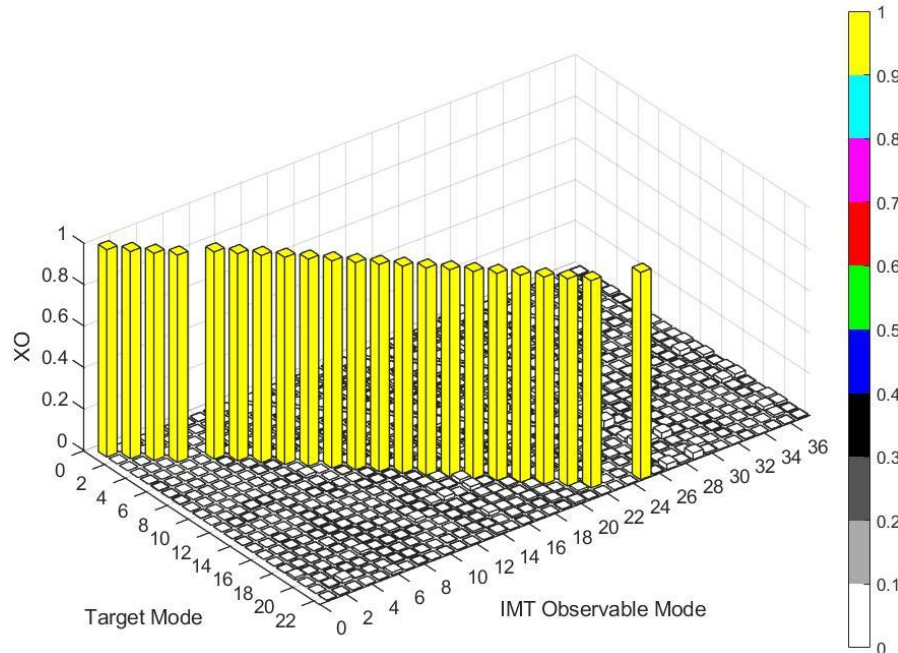
Figure 5.5-5. XO Between Target Modes and All Observable R4 IMT Modes Below 5.46 Hz

During each iteration of the MC analysis, the random system modes were uniquely matched to the nominal system modes. The random modes were then recovered at the sensor DOF and mass normalized with respect to the nominal TAM mass matrix. The XO between the random target modes and the random observable modes using the TAM mass matrix was computed and the largest off-diagonal magnitude for each target mode was retained. Figure 5.5-6 shows the nominal, median, and the P98/90 enclosure intervals for the maximum off-diagonal values for each target mode. All nominal values are below 0.037. For the most part, the median values are close to the nominal values. The P99/90 maximum off-diagonal values are less than 0.053 for all the target modes, except target mode 27, which is the SRB 2nd bending/CAA lateral bending mode. Figure 5.5-6 shows that the P99/90 value for mode 27 is much larger than both the nominal and median values, indicating that there is a large tail in the distribution of the maximum off-diagonal values. Figure 5.5-7 illustrates the corresponding cumulative distribution function for mode 27. Even though the P99/90 maximum off-diagonal value is greater than 0.25, there is still over a 92% probability that the maximum off-diagonal value is less than or equal to 0.10, which is often cited as the orthogonality criterion. These results indicate that during the actual IMT, there is high probability and confidence that the first 21 target modes can be separated from the observable modes below 5.46 Hz. In addition, there is a significant probability that target mode 27 can also be separated.
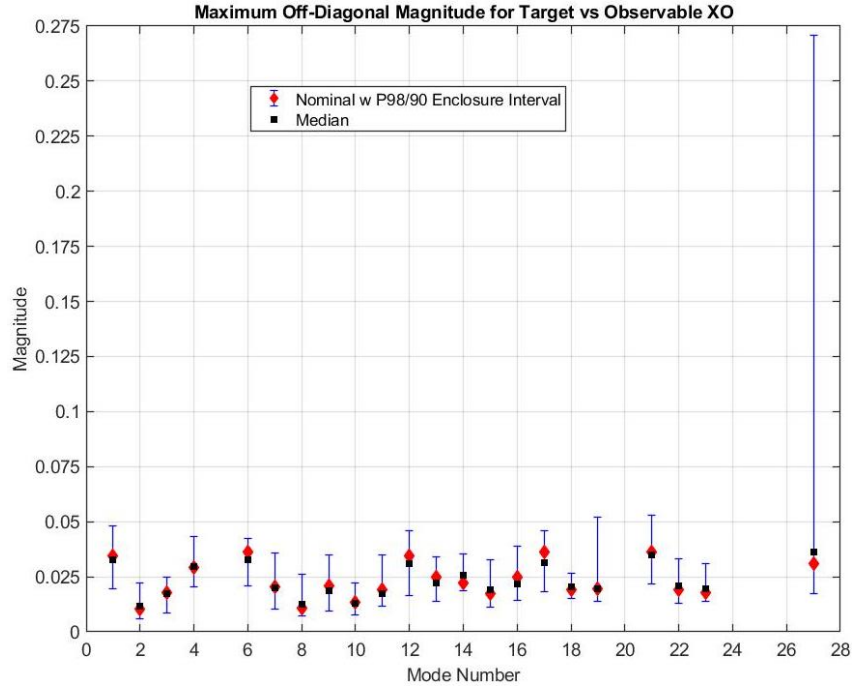
Figure 5.5-6. Maximum Off-Diagonal Statistics for XO Between Target and All Observable R4 IMT Modes Below 5.46 Hz
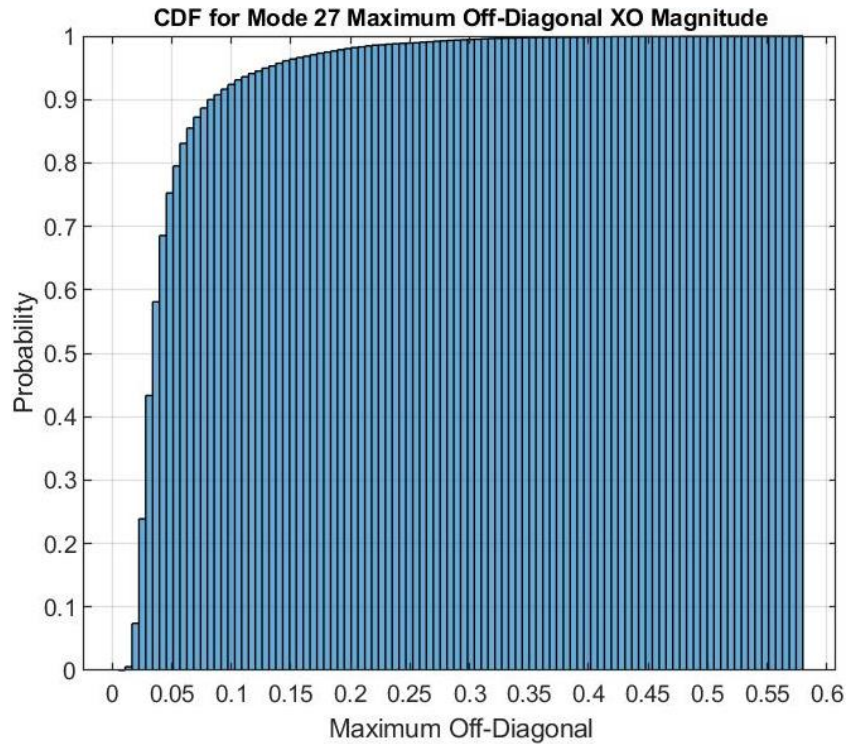
Figure 5.5-7. Cumulative Distribution Function for Maximum Off-Diagonal XO Between Target Mode 27 and All Observable R4 IMT Modes Below 5.46 Hz

Statistics were also computed for acceleration frequency response and mode indicator functions for the selected shaker and sensor configurations. A modal damping level of 1.0% and modes up to 16.0 Hz were included in the simulations. The shaker configuration selected for this

assessment corresponds to the configuration used in the two previous analyses, but with an additional two shakers, S32 and S40, as listed in Table 5.5-5. A typical acceleration frequency response at node 884 in the Y direction on the ICPS/LVSA due to input at shaker S36 is shown in Figure 5.5-8. The nominal and the P99/90 and P01/90 response levels are illustrated. During IMT posttest analysis, the corresponding test result can be compared with the predicted uncertainty interval shown in the figure. If the test result lies within the uncertainty interval, then confidence in the validity of the HPV UQ method is enhanced.

Table 5.5-5. IMT R4 Shaker Configuration

	Shaker Label	Node	Dir.	Location
1	S32	93038700	X	ML Zero Deck Vertical
2	S35	2812552	X	RSRB Surface Normal, -60 deg Off +Y on SRB CL
3	S36	650319	X	LH$_2$ Tank, +15 deg Off +Z Toward Core CL
4	S38	93579031	Y	ML Mid Tower
5	S40	93003115	Z	ML Zero Deck Vertical
6	S50	3002573	X	ML Pad, Top Deck Surface Normal
7	S51	3002292	Y	ML Pad, Top Deck Surface Parallel
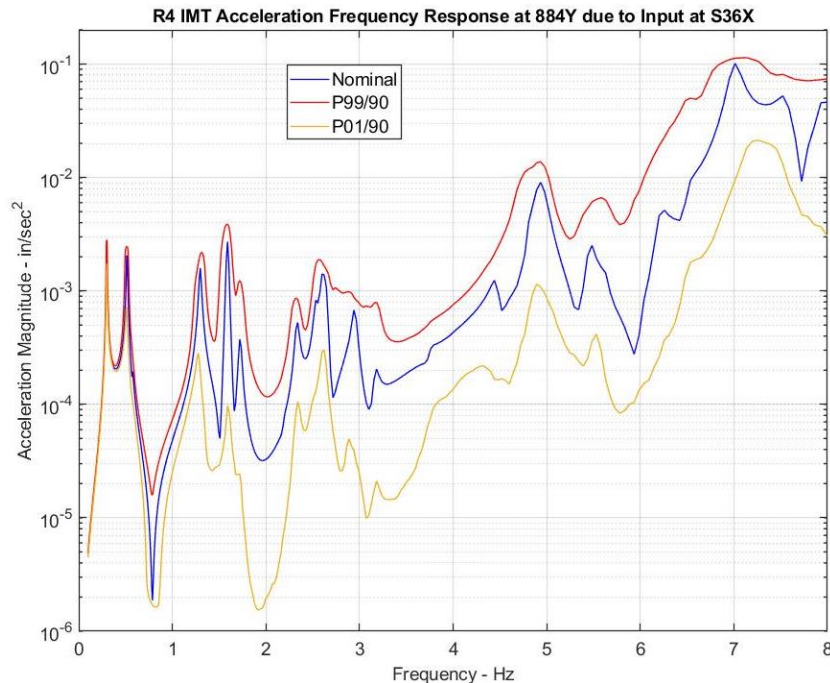
Figure 5.5-8. Acceleration Frequency Response at 884Y due to Input from Shaker S36 – IMT-UM3

The NMIF can be used to determine how effectively each of the primary target modes is excited and measured using the proposed shaker/sensor configuration. As mentioned previously, in practice an NMIF value of 0.3 or smaller indicates that the mode is sufficiently excited and measured to be extracted from the test frequency response data. Therefore, for a mode to be sufficiently excited and measured, it must have an NMIF value less than or equal to 0.30 for any of the shakers. Figure 5.5-9 illustrates the minimum NMIF value over all shakers for each of the primary target modes for the nominal system. The values were determined by evaluating the NMIF functions at the nominal target mode frequencies. As discussed previously, this approach

is conservative because the minimum of the NMIF does not typically occur at the resonance, so this approach does not always capture the true minimum value.
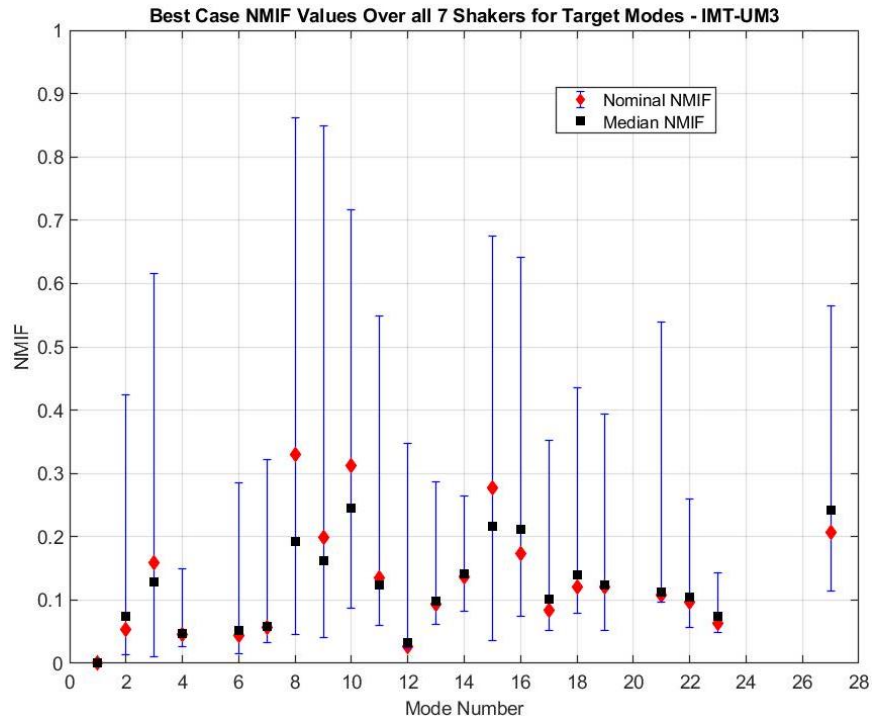
Figure 5.5-9. R4 IMT Primary Target Mode NMIF Statistics for seven Shakers – IMT-UM3

Using the criterion of NMIF being less than or equal to 0.30, 20 of the 22 primary R4 IMT target modes are sufficiently excited and measured using the proposed R4 shaker/sensor configuration. Figure 5.5-9 also shows the minimum P99/90 and P01/90 NMIF values for each target mode over all seven shakers. The NMIF values corresponding to the random systems are determined by uniquely matching each of the nominal system target modes to a random mode and then evaluating the random NMIF function at the corresponding random resonant frequency. It can be seen from Figure 5.5-9, that there is a significant amount of uncertainty in the NMIF values for all target modes except the first. The median values of the target mode NMIF values over the ensemble are also presented in Figure 5.5-9. In many cases, the median NMIF values are close to the nominal values. Applying the 0.30 criterion to the median NMIF values, the figure indicates that there is a 50% probability of identifying all of the target modes during the IMT. Seven of the target modes have P99/90 NMIF values less than 0.30.

As a comparison, the NMIF analysis was repeated for the original five shaker configurations listed in Table 5.3-2. Figure 5.5-10 illustrates the corresponding NMIF data. There are now four target modes with nominal NMIF values greater than the 0.30 threshold; modes 8 and 10 from the seven shaker case, and two additional modes, 7 and 16. The median NMIF values for modes 7, 8, and 16 are also greater than the threshold for the five shaker configuration. Figure 5.5-11 shows these results in a direct comparison of nominal and median NMIF values for the seven and five shaker configurations. The removal of shakers S32 and S40 has no impact on the target modes that pass the threshold at the P99/90 confidence level.
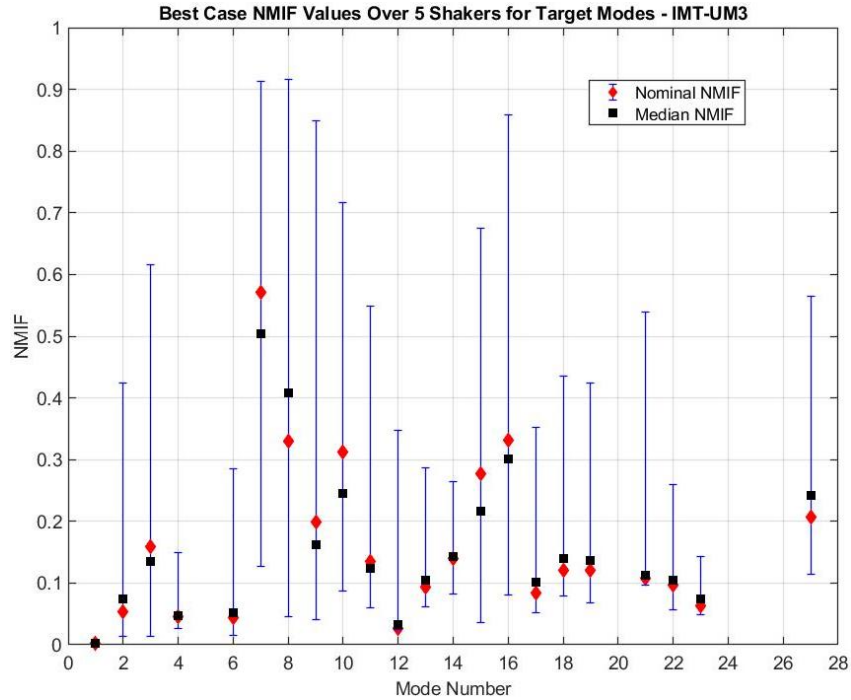
Figure 5.5-10. R4 IMT Primary Target Mode NMIF Statistics for Five Shakers – IMT-UM3
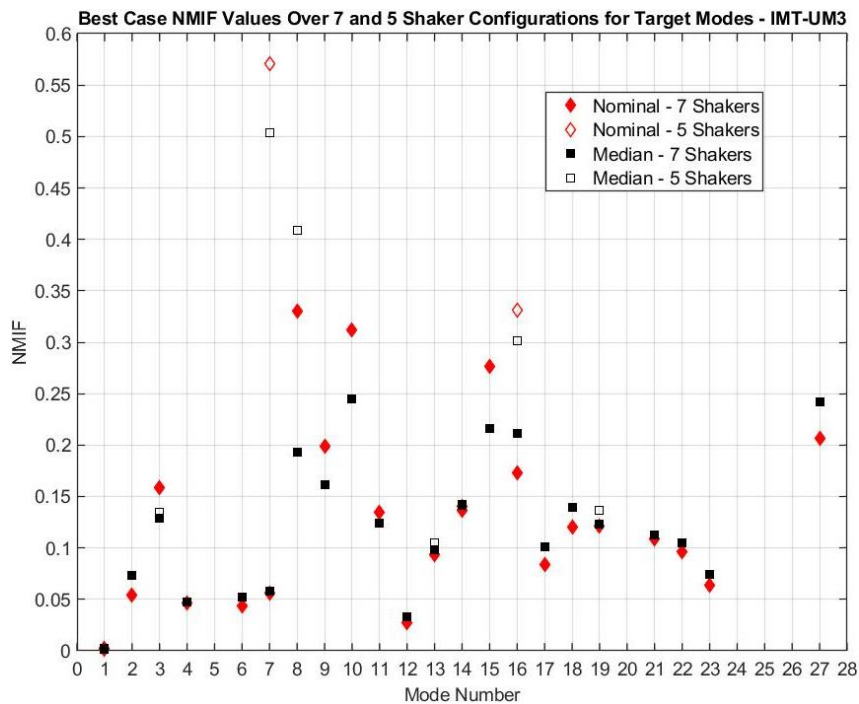
Figure 5.5-11. R4 IMT Primary Target Mode Nominal and Median NMIF for Seven and Five Shakers – IMT-UM3

5.6   Summary of Results

NASA has historically tested LVs in an integrated configuration with boundary conditions controlled to approximate the boundary conditions expected in flight. However, to minimize cost and schedule, a cross-program decision was made to not perform an IVGVT and rely on

analytical methods supported by component test results. However, there will still be an integrated system that will undergo testing, called the IMT. The IMT is a ground test of the integrated vehicle, assembled on the ML in VAB facility at KSC. The results of the IMT will provide an opportunity to validate or update previously correlated SLS component models such that, in an assembled configuration, they provide agreement with integrated system test results.

The purpose of this assessment was to apply the HPV UQ approach to the IMT/MSO ground vibration test configuration. Projection of component test-based uncertainty into the system provided estimates of the system-level uncertainty that can be expected in IMT target modal parameters (e.g., frequencies and mode shapes). Component uncertainty was also propagated into system-level acceleration frequency response and corresponding mode indicator functions. The HPV method combines a parametric variation of the HCB FI modal frequencies with an NPV method that randomly varies the HCB stiffness matrices as Wishart random matrix distributions using RMT. Uncertainty models were developed for each of the HCB components using the test-analysis correlation results from the component test-configuration modal tests. The component uncertainty was propagated to the system level using a MC approach that generated statistics for system-level results. This provided a UQ method that can be traced directly to available test data, and which can be updated as additional data and improved models become available.

Two cases were considered for the R3A IMT configuration during this assessment, the first included all component uncertainty models assigned based on component modal test results, 1

UQ analysis using uncertainty models for the two cases showed that the uncertainty in the ML dominates the uncertainty in the IMT configuration. If ML uncertainty is included in the system, the maximum RMS target mode frequency uncertainty was 23.06%. In contrast, if ML uncertainty is not included, the maximum RMS target mode frequency uncertainty was only 1.11%. The target mode shape uncertainty was likewise dramatically affected by ML uncertainty. The P01/90 value for the DCGM XO metric increased from 85.76 to 97.10 when ML uncertainty was not included in the system uncertainty model. If the IMT test-analysis correlation criteria for the target modes are frequency error less than or equal to 5.0% and an XO value greater than or equal to 0.90, then none of the 17 target modes would pass the XO criterion at the P01/90 level and seven of the 17 target modes would pass the frequency criterion at the P99/90 level for the assumed uncertain ML. In the case where there is no ML uncertainty, 14 of the 17 target modes would pass the XO criterion at the P01/90 level and all 17 target modes would pass the frequency criterion at the P99/90 level. In practice, a target mode is said to be correlated if the frequency and XO correlation criteria are passed at the same time. In the case of the uncertain ML, two of the 17 target modes are correlated in over 90% of the ensemble members, while in the case of no ML uncertainty, 15 of the 17 target modes pass the correlation criteria in over 99% of the ensemble members.

Statistics were computed for acceleration frequency response and mode indicator functions for the selected shaker and sensor configurations. A modal damping level of 1.0% and modes up to 16.0 Hz were included in the simulations. The XO between the primary target modes and the first 40 IMT modes below 5.11 Hz indicated that the target modes are decoupled from the other IMT modes using the R3A sensor configuration. A typical acceleration frequency response at node 860 in the Y direction on the ICPS/LVSA due to input at shaker S36 was computed for both uncertainty models. It was found that the uncertainty in the frequency response between 1.2

and 3.2 Hz was significantly higher when ML uncertainty was included. Above 3.2 Hz, the uncertainty in the selected frequency response for the two cases was approximately the same.

The NMIF can be used to determine how effectively each of the primary target modes is excited and measured using the sensor/shaker configuration—based on the fact that the real part of the frequency response becomes small near a resonance. Using the criterion of NMIF being less than or equal to 0.30, 16 of the 17 primary R3A IMT target modes are sufficiently excited and measured using the proposed sensor/shaker configuration. When ML uncertainty was present, it was found that there was a significant amount of uncertainty in the NMIF values for all of the target modes. In many cases, the median NMIF values were close to the nominal values. In the presence of ML uncertainty, applying the 0.30 criterion to the median NMIF values indicated there would be a 50% probability of identifying 15 of the 17 target modes during the IMT. Only one of the 17 target modes has a P99/90 NMIF value less than 0.30. When the ML has no uncertainty, several of the target mode NMIF values have significantly less uncertainty, while all NMIF values were less uncertain than when the ML was uncertain. For the most part, the median NMIF values were lower when there was no ML uncertainty.

The results of the R3A IMT UQ assessment indicate that if the ML model continues to improve prior to the IMT (i.e., the uncertainty is reduced) then the uncertainty in the IMT target modal parameters can be expected to be small, and the corresponding test-analysis correlation results should be adequate to indicate a correlated model. In addition, the probability of the target modes being accurately identified during the IMT will increase. While this assessment was completed prior to the IMT, during future posttest analysis, the test results can be compared to the UQ predictions. If the uncertainty predicted by the UQ analysis covers the test results, then there will be increased confidence that the HPV UQ method and the approach used to assign component uncertainty models are valid.

To be more consistent with future IMT test and analysis, a third UQ analysis was performed where the components were upgraded to the FRAC models that comprise the MSFC R4 IMT configuration. In addition, two shakers were added, the target mode set was changed to coincide with the R4 configuration, and the senor set was also updated. The FRAC ML component model was updated considerably over time based on component test results. Updated component uncertainty models were also generated based on the FRAC components. While the R4 IMT results are not directly comparable to the R3A results due to differences in target modes, shaker configurations, and sensor configurations, the overall uncertainty predicted for the R4 IMT configuration shows that the FRAC ML produces less uncertainty in the target modal parameters than the pretest ML, but more uncertainty than the certain ML, as expected.

During the R4 MC analysis, the maximum off-diagonal magnitude in the XO between the random target modes and the random observable modes using the TAM mass matrix was computed and tracked for each target mode. All nominal values were below 0.037. The P99/90 maximum off-diagonal values were less than 0.053 for all 22 target modes, except target mode 27, which is the SRB 2nd bending/CAA lateral bending mode. Even though the P99/90 maximum off-diagonal value was greater than 0.25, there was still over a 92% probability that the maximum off-diagonal value is less than or equal to 0.10, which is often cited as the orthogonality criterion. These results indicate that during the actual IMT, there is high probability and confidence that the first 21 of 22 target modes can be separated from the observable modes below 5.46 Hz. In addition, there is a significant probability that target mode 27 can also be separated.

Using the criterion of NMIF being less than or equal to 0.30, 20 of the 22 primary R4 IMT nominal target modes are sufficiently excited and measured using the proposed R4 seven-shaker/sensor configuration. Applying the 0.30 criterion to the median NMIF values, there is a 50% probability of identifying all 22 target modes during the IMT. Seven of the 22 target modes have P99/90 NMIF values less than 0.30. When shakers S32 and S40 are removed from the analysis, two additional target modes, 7 and 16, have nominal NMIF values greater than the 0.30 threshold, and three modes, 7, 8, and 16 have median values greater than the threshold. Therefore, shakers S32 and S40 have a significant positive impact on the identification of target modes 7, 8, and 16 during the IMT. While the results of this UQ evaluation provide meaningful insight into the effects of component uncertainty on system level results, the assessment was not meant to be a comprehensive UQ analysis of the SLS IMT. For simplicity, noteworthy sources of uncertainty (e.g. component damping) were neglected in this work. In future work, it is believed that the HPV approach can also be applied to the dispersion of the component damping matrix. Finally, while the HPV method provides a valuable tool for complex system UQ analysis using only a limited amount of data, it is believed that confidence in predicted results could be improved through a rigorous validation program.

6.0 Findings, Observations and NESC Recommendations

6.1 Findings

The following are specific findings from this work and are directed at the SLS Level 2 System Integration team:

F-1. Uncertainty in the ML dominates uncertainty in the IMT target mode parameters, frequency response, and mode indicator functions.

F-2. As uncertainty in the ML decreases, the uncertainty in the IMT target mode parameters becomes small, indicating that test-analysis correlation results should improve.

F-3. If the IMT test-analysis correlation criteria for the target modes are frequency error ≤5.0% and an XO value ≥0.90, then none of the target modes would pass the XO criterion at the P01/90 level and seven of the target modes would pass the frequency criterion at the P99/90 level for the uncertain pretest ML in the R3A configuration.

F-4. If the IMT test-analysis correlation criteria for the target modes are frequency error ≤5.0% and an XO value ≥0.90, then 14 of the target modes would pass the XO criterion at the P01/90 level and all of the target modes would pass the frequency criterion at the P99/90 level for an ML with no uncertainty in the R3A configuration.

F-5. In the presence of ML uncertainty in the R3A configuration, applying the 0.30 criterion to the median NMIF values indicated there would be a 50% probability of identifying 15 of the 17 target modes during the IMT. As the ML uncertainty decreases, the probability of identifying the target modes during the IMT increases.

F-6. Based on the R4 UQ analysis, there is high probability and confidence that the first 21 target modes can be separated from the observable modes below 5.46 Hz, and a significant probability that target mode 27 can also be separated during the IMT.

F-7. Based on the R4 UQ analysis, there is a 50% probability that the NMIF is less than 0.30 for all 22 of the target modes using all seven shaker locations.

F-8.   Based on the R4 UQ analysis, when shakers S32 and S40 are removed, there is a 50% probability that the normal mode indicator function is greater than 0.30 for target modes 7, 8, and 16 (i.e., shakers S32 and S40 significantly facilitate the identification of target modes 7, 8, and 16).

F-9.   The more accurate the ML model, the more likely the IMT will be successful.

6.2   Observations

The following observation was made during the course of this investigation:

O-1.   The HPV method provides a valuable tool for complex system UQ analysis using only a limited amount of component-based data. However, it is believed that confidence in predicted results could be improved through a rigorous analytical and experimental validation program.

O-2.   Using a multi-configuration approach for pre-test planning of the IMT has resulted in a test plan that is robust with respect to model uncertainty.

O-3.   It is necessary to have specific shakers located and oriented to be able to properly excite all of the target modes. This requires the ability to re-orient or relocate shakers to the needed locations.

O-4.   The UQ analysis performed for IMT includes test-based component uncertainty, but does not include uncertainty at the interfaces between components.

6.3   NESC Recommendations

The following are recommendations directed to the Exploration Systems Development/Cross-Program System Integration Office and the SLS System Analysis and Integration Office:

R-1.   The SLS System Analysis and Integration Office should incorporate a formal method (e.g., NPV and HPV discussed herein) for capturing model-form uncertainty prior to the FRAC for Artemis II and subsequent flights. *(F-1 to F-9)*

R-2.   Dynamic integrated SLS and element FEM UQ should be quantified by tying uncertainty to post Artemis I modal test results and subsequent future element testing, and reviewed at each flight's FRAC kickoff. *(F-1 to F-9)*

R-3.   To allow Artemis I IMT shaker re-orientation and re-location, appropriate support personnel (e.g., the hardware mechanics, the test team, etc.) should be available at times during IMT when transitions are being made. *(F-7, F-8, O-3)*

This recommendation has been designated as critical to the success of the IMT based on UQ results showing that seven shaker location/orientations are required to excite all the target modes, but only five shaker location/orientations will be implemented at one time during the IMT.

6.4   Future Work

Future work in the overall assessment will include another application of the HPV method to the IMT once the test data and the most current component models are available. The goal is to compute P99/90 test-analysis correlation metrics, frequency response, and mode indicator functions that can be compared with the corresponding metrics from the actual vibration test. If

the statistical results cover the actual test results, there will be increased confidence that the HPV UQ method and the approach used to assign component uncertainty models are valid. There will also be improved confidence that the flight component uncertainty models used in previous guidance, navigation, and control system stability analysis and the CLA were adequate.

7.0 Alternate Viewpoints

No alternate viewpoints were identified during the course of this assessment.

8.0 Other Deliverables

No unique hardware, software, or data packages, aside from those contained in this report, were disseminated to other parties outside this assessment.

9.0 Lessons Learned

No applicable lessons learned were identified for entry into the NASA Lessons Learned Information System analyses as a result of this assessment.

10.0 Recommendations for NASA Standards and Specifications

NASA currently does not have a standard for Uncertainty Quantification (UQ). The closest is NASA-STD-7009A, "Standard for Models and Simulations," July 13, 2016. This refers generically to uncertainty characterization in many locations, but does not address specific algorithms for quantifying uncertainty, or for accounting for the effect of model form on uncertainty. It is recommended that future NASA standards specify that UQ include the effect of model form, and that uncertainty be tied to available test results to the extent possible.

11.0 Definition of Terms

Finding	A relevant factual conclusion and/or issue that is within the assessment scope and that the team has rigorously based on data from their independent analyses, tests, inspections, and/or reviews of technical documentation.
Lessons Learned	Knowledge, understanding, or conclusive insight gained by experience that may benefit other current or future NASA programs and projects. The experience may be positive, as in a successful test or mission, or negative, as in a mishap or failure.
Observation	A noteworthy fact, issue, and/or risk, which may not be directly within the assessment scope, but could generate a separate issue or concern if not addressed. Alternatively, an observation can be a positive acknowledgement of a Center/Program/Project/Organization's operational structure, tools, and/or support provided.
Recommendation	A proposed measurable stakeholder action directly supported by specific Finding(s) and/or Observation(s) that will correct or mitigate an identified issue or risk.

12.0 Acronyms

CAA	Crew Access Arm
CAD	Computer Aided Design
CL	Centerline
CLA	Coupled Loads Analysis
CMIF	Complex Mode Indicator Function
CPIT	Cross-program Integration Team
CS	Core Stage
CSI	Cross-program Systems Integration
DCGM	Diagonal Cross-Generalized Mass
deg	Degree
DOF	Degree of Freedom
DTaMSS	Dynamic Test and Model Sensitivity Study
EGS	Exploration Ground System
EM-1	Exploration Mission 1
ESD	Exploration Systems Development
FDRA	Flight Dynamic Risk Assessment
FEM	Finite Element Model
FI	Fixed Interface
FRAC	Flight Readiness Analysis Cycle
GP	Gaussian Process
HCB	Hurty/Craig-Bampton
HEOMD	Human Exploration and Operations Mission Directorate
HPV	Hybrid Parametric Variation
Hz	Hertz
ICPS	Interim Cryogenic Propulsion Stage
IMT	Integ2wrated Modal Test
IMT-UM	Integrated Modal Test Uncertainty Model
ISPE	Integrated Spacecraft Payload Element
IVGVT	Integrated Vehicle Ground Vibration Test
JLTT	Joint Loads Task Team
KSC	Kennedy Space Center
L&D	Loads and Dynamics
LAS	Launch Abort System
LH_2	Liquid Hydrogen
LSRB	Left Solid Rocket Booster
LV	Launch Vehicle
LVSA	Launch Vehicle Stage Adapter
MC	Monte Carlo
MEM	Modal Effective Mass
ML	Mobile Launcher
MPCV	Multipurpose Crew Vehicle
MSA	MPCV Spacecraft Adaptor
MSFC	Marshall Space Flight Center
MSO	Mass Simulator for Orion
NESC	Nasa Engineering Safety Center

NMIF	Normal Mode Indicator Function
NPV	Nonparametric Variation
NRB	NESC Review Board
psi	Pounds per Square Inch
RMS	Root Mean Square
RMT	Random Matrix Theory
RSRB	Right Solid Rocket Booster
RSS	Root Sum Square
RV	Residual Vector
SLS	Space Launch System
SRB	Solid Rocket Booster (Solid Rocket Motor)
TAM	Test Analysis Model
TDT	Technical Discipline Team
UM	Uncertainty Model
UQ	Uncertainty Quantification
VAB	Vertical Assembly Building
VAC-1	Vehicle Analysis Cycle 1
XO	Cross-Orthogonality

13.0   References

1.   Sills, J.; Blelloch, P.; and Kammer, D.: *Uncertainty Propagation for Model Validation Subtask*, NESC-TI-16-01110 UQ RP V.2.0, January 2020.

2.   Wishart, J.: "Generalized Product Moment Distribution in Samples," *Biometrika,* vol. 20A, no. 1-2, pp. 32-52, 1928.

3.   Rades, M.: "Performance of Various Mode Indicator Functions," *Shock and Vibration*, vol. 17, 473–482, 2010.

4.   Kammer, D.; Blelloch, P.; and Sills, J.: "Test-Based Uncertainty Quantification and Propagation Using Hurty/Craig-Bampton Substructure Representations," in *IMAC*, Orlando, FL, 2019.

5.   Kammer, D.; Blelloch, P.; and Sills, J.: "Variational Coupled Loads Analysis using the Hybrid Parametric Variation Method," in *IMAC*, Houston, TX, 2020.

6.   Soize, C.: "A Nonparametric Model of Random Uncertainties for Reduced Matrix Models in Structural Dynamics," *Probabilistic Engineering Mechanics,* vol. 15, no. 3, pp. 277-294, 2000.

7.   Soize, C.: "Maximum Entropy Approach for Modeling Random Uncertainties in Transient Elastodynamics," *J. Acoust. Soc. Am.,* vol. 109, no. 5, pp. 1979-1996, 2001.

8.   Adhikari, S.: "Wishart Random Matrices in Probabilistic Structural Mechanics," *J. Eng. Mech.,* vol. 134, no. 12, pp. 1029-1044, 2008.

9.   Capiez-Lernout, E.; Pellissetti, M.; Pradlwarter, H.; Schueller, G. I.; and Soize, C.: "Data and model uncertainties in complex aerospace engineering systems," *J. Sound Vib.,* vol. 295, no. 3-5, p. 923–938, 2006.

10. Gramacy, R.: *Surrogates, Gaussian Process Modeling, Design, and Optimization for the Applied Sciences*, CRC Press, Boca Raton, FL, 2020.

11. Blelloch, P.: "Cross-Orthogonality of Closely Spaced Modes," in *IMAC*, 2006.

12. Kabe, A.; and Sako, B.: *Structural Dynamics Fundamentals and Advanced Applications – Volume 2*, Elsevier Science, June 2020.

Appendix A.

Table A-1. IMT R3A Sensor Set

Node	Dir.	Location	Node	Dir.	Location	Node	Dir.	Location
860	2	ICPS/LVSA	1863874	1	LSRB	3200110	2	ML
884	2	ICPS/LVSA	1876815	3	LSRB	3200178	2	ML
609505	3	CS	2303245	13	ICPS/LVSA	3200600	2	ML
610012	2	CS	2303341	13	ICPS/LVSA	3200601	2	ML
610068	2	CS	2800901	2	RSRB	3200602	2	ML
610093	23	CS	2800931	2	RSRB	3200604	12	ML
611601	3	CS	2801041	2	RSRB	3200605	3	ML
611602	23	CS	2801440	2	RSRB	3200607	23	ML
620100	2	CS	2801712	3	RSRB	3200608	2	ML
641027	3	CS	2801980	1	RSRB	3200610	3	ML
650035	2	CS	2802072	1	RSRB	3200611	3	ML
650243	12	CS	2812738	1	RSRB	3200612	2	ML
650252	1	CS	2812886	1	RSRB	3200614	2	ML
650331	1	CS	2812946	2	RSRB	3200621	23	ML
650515	1	CS	2813022	2	RSRB	3200623	2	ML
651807	2	CS	2813098	12	RSRB	3200624	3	ML
651819	2	CS	2813126	1	RSRB	3200627	3	ML
651822	1	CS	2813399	1	RSRB	3200630	23	ML
651868	1	CS	2813519	1	RSRB	3200635	2	ML
651975	2	CS	2813607	1	RSRB	3200636	13	ML
652168	3	CS	2820042	1	RSRB	3200638	3	ML
669070	3	CS	2820134	1	RSRB	3200639	2	ML
671310	2	CS	2820522	1	RSRB	3200641	1	ML
682241	2	CS	2828191	2	RSRB	3200642	23	ML
682274	2	CS	2828329	1	RSRB	3200643	2	ML
682329	2	CS	2828358	2	RSRB	3200644	3	ML
690227	3	CS	2840005	1	RSRB	3200650	3	ML
691017	3	CS	2840093	1	RSRB	3200651	3	ML
691807	123	CS	2840485	3	RSRB	3200652	3	ML
1800901	12	LSRB	2840513	2	RSRB	3200655	3	ML
1800931	1	LSRB	2840545	12	RSRB	3200656	1	ML
1801091	2	LSRB	2840573	1	RSRB	3200658	2	ML
1801289	3	LSRB	2856924	2	RSRB	3200659	123	ML
1801381	3	LSRB	2856935	2	RSRB	3200660	2	ML
1801712	3	LSRB	2856942	2	RSRB	3200662	3	ML
1801740	3	LSRB	2856970	2	RSRB	3200663	12	ML
1812858	1	LSRB	2858967	2	RSRB	3200688	3	ML
1812886	1	LSRB	2859011	2	RSRB	3200739	3	ML
1813069	1	LSRB	2859764	2	RSRB	3200754	3	ML
1813086	2	LSRB	2859792	3	RSRB	3400029	2	ML
1813098	1	LSRB	2861008	2	RSRB	3410016	2	ML

1813126	1	LSRB	2861024	2	RSRB	3410018	1	ML
1813367	1	LSRB	2861052	2	RSRB	3430243	3	ML
1813459	1	LSRB	2863050	2	RSRB	3432109	1	ML
1813607	1	LSRB	2863065	2	RSRB	3432110	3	ML
1820466	1	LSRB	2863874	1	RSRB	3432133	2	ML
1820483	2	LSRB	3000109	1	ML	3522607	3	ML
1820494	1	LSRB	3000126	1	ML	3525974	1	ML
1820522	1	LSRB	3000250	1	ML	3555970	3	ML
1827607	1	LSRB	3000989	2	ML	3555974	1	ML
1828184	1	LSRB	3001093	1	ML	71105563	2	CS
1828186	12	LSRB	3001166	2	ML	71343594	3	CS
1828330	1	LSRB	3002531	1	ML	71344893	12	CS
1840033	1	LSRB	3003289	2	ML	72105379	2	CS
1840485	3	LSRB	3003300	1	ML	72344893	1	CS
1840513	3	LSRB	3003311	2	ML	73105563	2	CS
1840545	12	LSRB	3003357	13	ML	73344893	12	CS
1840573	12	LSRB	3003411	13	ML	74105379	2	CS
1856911	2	LSRB	3003457	3	ML	74344893	12	CS
1856925	2	LSRB	3005349	13	ML	90600041	13	CS
1856941	2	LSRB	3009616	123	ML	90649801	12	CS
1856942	1	LSRB	3013057	23	ML	90649802	2	CS
1856970	1	LSRB	3017669	1	ML	90649803	2	CS
1859011	2	LSRB	3022552	2	ML	90687405	13	CS
1859764	2	LSRB	3026416	123	ML	90687406	2	CS
1859792	3	LSRB	3030916	12	ML	93003172	2	ML
1861008	2	LSRB	3033797	1	ML	94234112	2	MSO/MSA
1861024	2	LSRB	3035719	3	ML	94300375	23	MSO/MSA
1861052	2	LSRB	3038097	123	ML	94300818	2	MSO/MSA
1863065	2	LSRB	3038127	123	ML	94317497	2	MSO/MSA
1863093	2	LSRB	3055213	3	ML	94318293	2	MSO/MSA

Table A-2. IMT R4 Sensor Set

Node	Dir.	Location	Node	Dir.	Location	Node	Dir.	Location
884	2	ICPS/LVSA	2813098	12	RSRB	3200608	2	ML
610068	2	CS	2813126	1	RSRB	3200610	3	ML
611601	3	CS	2813399	1	RSRB	3200611	23	ML
611602	23	CS	2813519	1	RSRB	3200612	23	ML
641027	3	CS	2813607	1	RSRB	3200621	3	ML
650243	12	CS	2820042	1	RSRB	3200627	3	ML
650252	1	CS	2820134	1	RSRB	3200630	2	ML
650331	1	CS	2820522	1	RSRB	3200631	2	ML
650443	1	CS	2828193	2	RSRB	3200635	2	ML
651807	2	CS	2828358	2	RSRB	3200636	13	ML
651819	2	CS	2840005	1	RSRB	3200638	3	ML
651975	2	CS	2840093	1	RSRB	3200639	2	ML
671310	1	CS	2840485	3	RSRB	3200642	3	ML
682274	123	CS	2840513	2	RSRB	3200643	3	ML
734749	2	ICPS/LVSA	2840545	12	RSRB	3200644	3	ML
1801712	3	LSRB	2840573	1	RSRB	3200650	3	ML
1802401	2	LSRB	2856924	2	RSRB	3200652	3	ML
1812531	12	LSRB	2856935	2	RSRB	3200655	3	ML
1812557	3	LSRB	2856942	2	RSRB	3200656	1	ML
1812858	1	LSRB	2858967	2	RSRB	3200658	2	ML
1812886	1	LSRB	2859011	2	RSRB	3200660	2	ML
1813069	1	LSRB	2859764	2	RSRB	3200662	1	ML
1813086	2	LSRB	2859792	3	RSRB	3200663	2	ML
1813098	1	LSRB	2861008	2	RSRB	3200726	3	ML
1813126	1	LSRB	2861052	2	RSRB	3200728	2	ML
1813459	1	LSRB	2863050	2	RSRB	3200739	3	ML
1813607	1	LSRB	2863874	1	RSRB	3200754	3	ML
1820466	1	LSRB	3000109	1	ML	3201594	2	ML
1820483	2	LSRB	3000126	1	ML	3202784	2	ML
1820494	1	LSRB	3000250	1	ML	3400029	2	ML
1820522	1	LSRB	3001093	1	ML	3410016	2	ML
1828186	2	LSRB	3001180	2	ML	3410017	1	ML
1828330	1	LSRB	3001372	1	ML	3410019	3	ML
1840033	1	LSRB	3001468	3	ML	3420020	2	ML
1840513	3	LSRB	3002292	2	ML	3432109	1	ML
1840545	12	LSRB	3002531	1	ML	3432110	3	ML
1840573	1	LSRB	3002573	3	ML	3522607	3	ML
1856911	2	LSRB	3003072	1	ML	3525974	1	ML
1856941	2	LSRB	3003075	1	ML	3551835	1	ML
1856942	1	LSRB	3003300	1	ML	3555970	3	ML

1856970	1	LSRB	3003311	2	ML	3750337	3	ML
1859011	2	LSRB	3003357	1	ML	71105563	2	CS
1859764	2	LSRB	3003411	3	ML	72105379	2	CS
1861024	2	LSRB	3003457	3	ML	73105563	2	CS
1863065	2	LSRB	3005349	1	ML	74105379	2	CS
1863093	2	LSRB	3026416	12	ML	74344893	12	CS
1863874	1	LSRB	3030916	12	ML	90600041	3	CS
1876815	3	LSRB	3038097	23	ML	90610282	1	CS
2801041	2	RSRB	3038127	13	ML	90649801	2	CS
2801712	3	RSRB	3200129	1	ML	90649803	1	CS
2801980	1	RSRB	3200169	2	ML	93003115	23	ML
2802072	1	RSRB	3200170	2	ML	93003172	12	ML
2802401	2	RSRB	3200495	3	ML	94297917	2	MSO
2802431	2	RSRB	3200503	3	ML	94300818	2	MSO
2812552	13	RSRB	3200544	1	ML	94306841	2	MSO
2812738	1	RSRB	3200600	2	ML	95303245	123	ICPS/LVSA
2812886	1	RSRB	3200602	12	ML			
2812946	2	RSRB	3200604	12	ML			

REPORT DOCUMENTATION PAGE

1. REPORT DATE *(DD-MM-YYYY)*	2. REPORT TYPE	3. DATES COVERED *(From - To)*
02/03/2021	Technical Memorandum	

4. TITLE AND SUBTITLE

NESC Peer Review of Exploration Systems Development (ESD) Integrated Vehicle Modal Test, Model Correlation, Development Flight Instrumentation (DFI) and Flight Loads Readiness

Uncertainty Propagation for Model Validation Sub-task

5a. CONTRACT NUMBER

5b. GRANT NUMBER

5c. PROGRAM ELEMENT NUMBER

6. AUTHOR(S)

Sills, Joel; Blelloch, Paul; Kammer, Daniel

5d. PROJECT NUMBER

5e. TASK NUMBER

5f. WORK UNIT NUMBER
869021.01.23.01.01

7. PERFORMING ORGANIZATION NAME(S) AND ADDRESS(ES)
NASA Langley Research Center
Hampton, VA 23681-2199

8. PERFORMING ORGANIZATION REPORT NUMBER
NESC-RP-16-01110

9. SPONSORING/MONITORING AGENCY NAME(S) AND ADDRESS(ES)
National Aeronautics and Space Administration
Washington, DC 20546-0001

10. SPONSOR/MONITOR'S ACRONYM(S)
NASA

11. SPONSOR/MONITOR'S REPORT NUMBER(S)
NASA/TM-20210009733

12. DISTRIBUTION/AVAILABILITY STATEMENT
Unclassified - Unlimited
Subject Category Space Transportation and Safety
Availability: NASA STI Program (757) 864-9658

13. SUPPLEMENTARY NOTES

14. ABSTRACT
This report details a sub-task (regarding Uncertainty Propagation for Model Validation) from a NASA Engineering and Safety Center assessment that is a multi-year activity spanning the complete development of the Space Launch System integrated vehicle structural dynamic models, and the development of the certification of flight readiness for the Artemis 1 and Artemis 2 vehicles and their variants.

15. SUBJECT TERMS

Exploration Systems Development; Development Flight Instrumentation; Flight Loads Readiness; Uncertainty Quantification; NASA Engineering and Safety Center

16. SECURITY CLASSIFICATION OF:			17. LIMITATION OF ABSTRACT	18. NUMBER OF PAGES	19a. NAME OF RESPONSIBLE PERSON
a. REPORT	b. ABSTRACT	c. THIS PAGE			STI Help Desk (email: help@sti.nasa.gov)
U	U	U	UU	71	19b. TELEPHONE NUMBER *(Include area code)* (443) 757-5802